8-1-1999

Signiture analysis of fetal blood velocity waveforms

Ronald Soule

SIGNATURE ANALYSIS OF FETAL BLOOD VELOCITY WAVEFORMS

by

Ronald Soule

A Thesis Submitted
in
Partial Fulfillment
of the
Requirement for the

MASTER OF SCIENCE
in
MECHANICAL ENGINEERING

Approved by:

Professor Mark H. Kempski
Department of Mechanical Engineering _____
(Thesis Advisor)

Dr. Risa J. Robinson
Department of Mechanical Engineering _____
(Committee Member)

Dr. Alan H. Nye
Department of Mechanical Engineering _____
(Committee Member)

Professor Charles W. Haines
Department of Mechanical Engineering _____
(Head of Department)

DEPARTMENT OF MECHANICAL ENGINNERING
ROCHESTER INSTITUTE OF TECHNOLOGY

August 1999

ABSTRACT

SIGNATURE ANALYSIS OF FETAL BLOOD VELOCITY WAVEFORMS

By
Ronald Soule

Thesis Advisor: Professor Mark H. Kempski

Doppler blood velocity waveform analysis is conducted to affect clinical diagnosis. Current analysis codes developed at RIT posses the capability to assess gross hemodynamic parameters such as heart rate, mean pulse velocity, peak systolic velocity and also the beat to beat variability of these parameters. These computer algorithms have, however, lacked the ability to determine hemodynamic indices such as the pulsatility and resistance index as well as the AB ratio. This latter deficiency stems from an algorithmic need to accurately determine end diastolic velocity in every cardiac cycle. The current thesis specifically augments current algorithms to accurately compute end diastolic velocity. The end diastolic velocity, peak systolic velocity and mean pulse velocity determined in each cardiac cycle are then used to compute the various pulse-velocity waveform indices noted above. In addition, the use of end diastolic velocity in conjunction with peak systolic velocity allows the velocity waveform to be dissected into diastolic subsections, which resemble decaying exponential curves. These exponential decay curves will be characterized via curve fitting. The goal of this thesis is to assess whether traditional pulsatility indices and/or the decay curve parameters are adequate to assess fetal developmental age between 10 - 13 weeks gestation. Discrimination assessment is conducted using neural network analysis techniques. Whether entire pulse-

velocity waveforms extracted between successive end-diastolic velocities provides a more robust data set for gestational age discrimination is also explored. The results suggest that hemodynamic indices computed for fetuses between 10 to 13 weeks gestation provide insufficient data for effective neural network classification. Use of the entire pulse-velocity waveform data in neural network analysis showed better fetal gestational age classification than use of waveform indices. However, similarity of waveforms between 10 – 13 weeks gestation prevented robust classification using either hemodynamic indices or entire pulse-velocity waveforms based on the fetal data records used for this study.

PERMISSION

I, Ronald Soule, hereby grant permission to the Wallace Memorial Library of the Rochester Institute of Technology to reproduce my thesis entitled ***Signature analysis of Fetal Blood Velocity Waveforms*** in whole or in part. Any reproduction will not be for commercial use or profit.

_____

Ronald Soule

Dedication

This thesis is dedicated to my parents, who's perpetual encouragement gave me the strength to fulfill my dreams.

and to

Dr. Kempski, the insight and kindness you have shown to me is evident in everything that I succeeded in at RIT.

TABLE OF CONTENTS

Chapter 1 Introduction

1.1 Cardiovascular Malformations

In the United States, eight in every 1000 infants are born with congenital circulatory problems (Clark and Takao, 1990). Throughout development there are numerous occasions for problems to arise, ranging from genetic disorders to environmentally induced malformations. As the fetus develops the heart begins to beat at approximately three weeks of gestation. As the heart continues to pump blood throughout the developing fetus, changes in the organ occur which begin a transition from a single heart tube to a four chambered organ several weeks later (Sissman, 1970). The 10 –13 week of gestation is a critical time of transition when morphometric problems have a greater chance to develop (Clark and Takao, 1990), with ensuing functional consequences later in gestation or postpartum.

A majority of malformations and, perhaps, adult cardiovascular disease occur during morphogenesis (Clark and Takao, 1990). The malformations lead to many atypical cardiovascular problems, which in the extreme cause cardiovascular system failure and fetal death (Clark and Takao, 1990). Hence, early detection of cardiac malformations and or cardiovascular system compromise is essential for proper obstetric care and treatment.

1.2 Velocity Waveform Index Correlation to Disease

The presence of development related cardiovascular malformations in the late-gestational fetus can be revealed through Doppler blood velocity waveform analysis (Evans *et al*, 1989). Specific waveform characteristics may therefore facilitate fetal cardiovascular health assessment. Typical waveform characteristics documented in the literature include peak-systolic velocity, end-diastolic velocity and mean pulse-velocity as well as derived indices such as the pulsatility index (PI), the AB ratio, and Pourcelot's resistance index (RI) which are associated with vascular impedance to flow (Thompson *et al*, 1986). One of the most common uses for the PI is the evaluation of proximal stenosis in peripheral arteries (Thompson *et al*, 1986), while both the PI and AB ratio have been used to assess peripheral vascular impedance levels (Thompson and Trudinger, 1986). Additionally the PI shows specificity to health analyses of intrauterine growth retardation (Laurin *et al*, 1987), during mid to late gestation.

Routine obstetric fetal monitoring throughout gestation has demonstrated that umbilical artery blood flow velocity is very informative when assessing the presence of increased placental resistance indicative of intrauterine growth retardation and pre-eclampsia (Surat and Adamson, 1996). In the third trimester of gestation the Doppler velocity waveform shows signs of decreased velocity between the peak-systolic velocity (S) and the end-diastolic velocity (D) (Thompson and Trudinger, 1989). Analysis has depicted that the cardiovascular system of the fetus can adapt to an increased placental resistance through an increase in cardiac contractility (Thompson and Trudinger, 1989).

Clinical obstetric Doppler blood velocity measurements often scrutinize the umbilical artery blood flow velocity because of the robust structure and health condition

of this blood vessel. Structurally the umbilical artery is long and un-branched which precludes the velocity waveform from becoming overly complex due to branching induced pressure wave reflections (Thompson and Stevens, 1989). Another positive aspect of the umbilical artery is that it is free of degenerative diseases, which could bias measurements intended to assess fetal and/or placental function (Thompson and Stevens, 1989). Likewise, invasive procedures are not required on the maternal-fetal pair since the cord is free floating and outside the body of the fetus *in utero* and readily monitored using clinical Doppler sonography techniques.

Routine fetal health evaluations are conducted between 15 to 20 weeks gestation, from 20 weeks to full term, as well as post partum for neonates, using Doppler blood velocity waveform data. In particular, during the third trimester, pregnancy induced hypertension reduces diastolic flow velocity (Thompson and Trudinger, 1989), and thus changes the shape of the Doppler velocity waveform. The analysis of velocity waveform characteristic indices (PI, RI, and AB ratio) have provided quantifiable evidence that these indices correspond to health and disease (Thompson *et al*, 1989). Herein values of the PI have been recorded in the range of 0.5 to 1.5 for normal pregnancies and can be upwards of 3 and higher for abnormal pregnancies (Thompson and Trudinger, 1989).

Furthermore, late gestational Doppler velocity waveform characteristic indices clearly show the presence of various cardiac malformations, which may be detected through altered PI, RI, and AB ratio values from nominal. However not all Doppler velocity waveform characteristic indices are sensitive to the presence of chronic and acute placental insufficiencies (Joern *et al*, 1997).

1.3 Thesis Objective

The current study seeks to determine the viability of the PI, RI, and AB ratio indices to assess fetal age and (ultimately) health during early gestation. The study will specifically address weeks 10 through 13 of pregnancy. The majority of work available in the literature has been consumed with the correlation of disease to Doppler velocity waveform indices in the mid to late gestational period (Joern *et al*, 1997). However it is necessary to develop evaluation criteria for early gestational fetuses since early detection is crucial for effective treatment of certain pathologies, including pre-eclampsia and intrauterine growth retardation (Thompson and Trudinger, 1989).

The aim of this thesis is to document whether various Doppler velocity waveform indices applied to fetal umbilical artery waveforms obtained early in gestation can be used to discriminate fetal age during the critical development period between 10 to 13 weeks gestation. Placental network functioning undergoes drastic changes following this time frame which will, in a large part, determine whether intrauterine growth retardation and or pre-eclampsia is likely later in gestation (Clark and Takao, 1990). Since waveform indices represent a condensation of velocity waveform time series data, and hence information loss, we will also scrutinize the pulse-velocity waveform. This latter scrutiny will be used to assess whether waveform indices for early gestational fetuses lack specificity for fetal age discrimination versus pulse-velocity waveform analysis.

The long-term aim of our investigation is the formulation of fetal velocity waveform discrimination criteria, which will aid clinical diagnosis of intrauterine growth retardation and pre-eclampsia prone maternal-fetal pairs and subsequent treatment. Our approach will start from scrutiny of a fetal pulse-velocity wave train obtained through

Doppler sonography records (Kempski *et al*, in review and Ursem *et al*, 1998). Each pulse velocity will be further distilled using descriptive pulse-velocity waveform indices such as the pulsatility index, the resistance index, the AB ratio, and a diastolic decay constant (τ) defined herein. Lastly neural network analysis will be used to assess the age and health discrimination potential of these indices as well as fetal-representative pulse-velocity waveforms between 10 to 13 weeks gestation.

Chapter 2 Methodology

2.1 Velocity Waveform Definition and Evaluation

2.1.1 Pulse-Velocity Waveform Definition

To calculate the PI, RI, the AB ratio and the diastolic decay constant (τ), the end-diastolic velocity (D), the peak-systolic velocity (S) and the mean pulse-velocity (M) need to be ascertained for each velocity pulse (Figure 2.1). The "peak-valley detection" algorithm (PVD) written in LabVIEW (National Instruments, Corporation, Austin Texas) performs these operations to increase speed and accuracy of the calculations, while removing human error in determining the values of the PI, RI, the AB ratio, and the diastolic decay constant (τ).

In order to select the end-diastolic velocity (D) in each pulse-velocity waveform and disregard all the other points, the velocity waveform is examined from pulse to pulse, sequentially using common "landmarks" for PVD data extraction. The first landmark used by the PVD algorithm is the global mean velocity ($\overline{M}$) computed across the entire velocity time series (Figure 2.1). Here $\overline{M}$ represents the average velocity such that individual pulse-velocity waveforms possess peak-systolic values (S) greater than $\overline{M}$ and end-diastolic value (D) less than $\overline{M}$. The mean pulse-velocity (M) for any individual pulse-velocity waveform may be either greater than or less than the global mean velocity $\overline{M}$. Next the peak systolic velocity (S) in each pulse-velocity waveform is found by using the "mean-crossing points" where the pulse-velocity "crosses" the value defined by the global mean $\overline{M}$ (Figure 2.1). Such crossings occur on the upward slope and the downward slope of a given pulse-velocity trace as seen in Figure 2.1. Pulse-velocity data

between the "mean-crossing points" are then searched for the maximum pulse-velocity value, thus defining the peak systolic pulse-velocity (S) and its temporal location within the velocity record (Figure 2.1). Once each peak pulse-velocity value is determined, the velocity wave train is re-segmented between every two consecutive systolic peak-velocities in order to determine respective end-diastolic velocity values (D) and their temporal location within the velocity record. However, before the end-diastolic velocity (D) can be found for each pulse-velocity, its definition needs to be established.

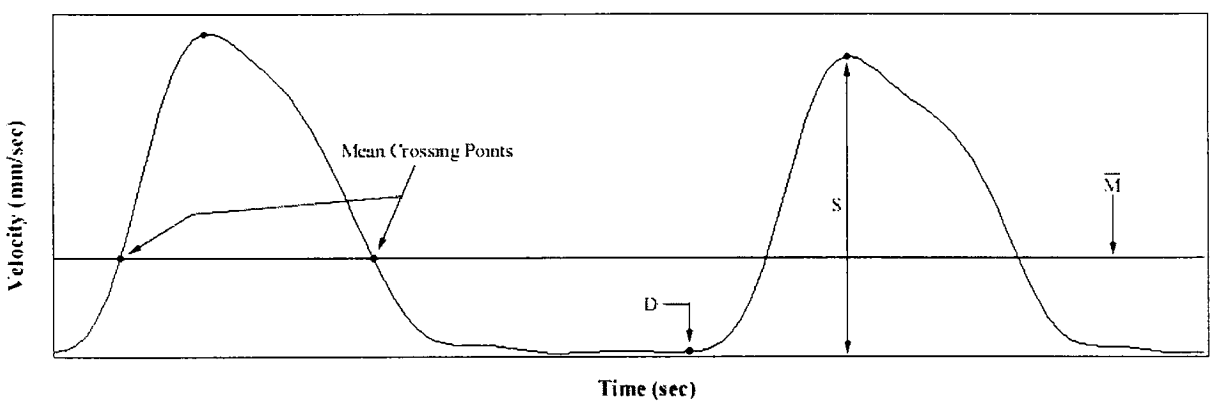

Figure 2.1 Plot of two consecutive cycles, describing the extraction of the peak-systolic point.

In each cardiac cycle the heart contracts thereby accelerating the blood flow velocity at the beginning of each cycle.

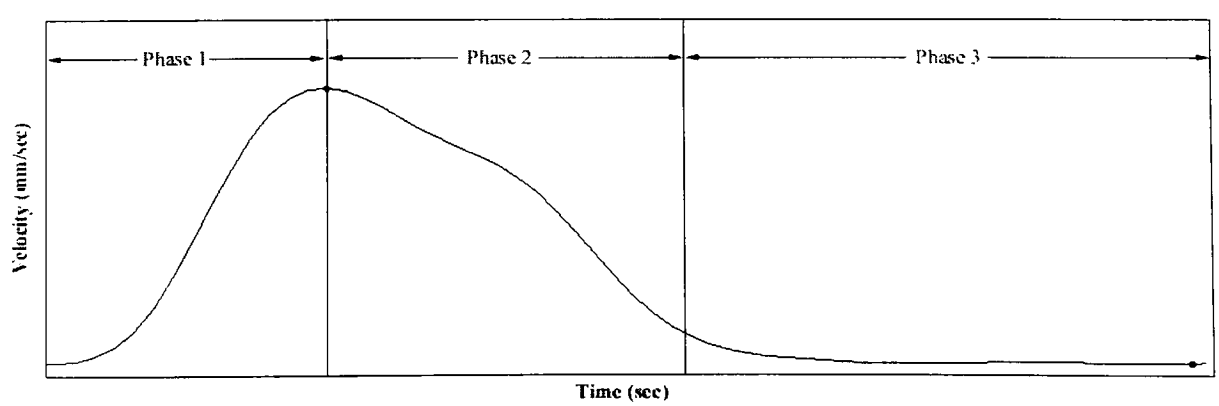

Figure 2.2 Depicts a "phasic" scrutiny of a representative pulse-velocity waveform.

Phase 1 depicted in Figure 2.2 is the distal vascular manifestation of cardiac contraction and initial ejection of blood from the left ventricle. Phase 2, depicted in Figure 2.2 starts at peak-systolic velocity and continues to include the distal vascular manifestations of ventricular relaxation and aortic valve closure. During phase 2 active ventricular ejection ceases, but flow continues due to capacitive discharge in the large arteries distal to the heart. Phase 3 in Figure 2.2 is the distal vascular manifestation of ventricular refilling prior to ventricular contraction during the succeeding cardiac cycle (Marieb, 1991). Therefore according to Figure 2.2 the end diastolic velocity (D) occurs at the juncture between phase 1 and phase 3. Thus D is the point where one cardiac cycle ends and the next begins.

The calculation of the end diastolic velocity (D) is attained in four steps. The first is the acquisition of pulse-velocity waveform data between successive peak-systolic velocities as shown in Figure 2.3. Step 2 invokes algorithm sub-routines to determine which points of the pulse-velocity waveform have a slope of $-1 < m < 1$, which are calculated from the first derivative of the pulse-velocity waveform. Next the second

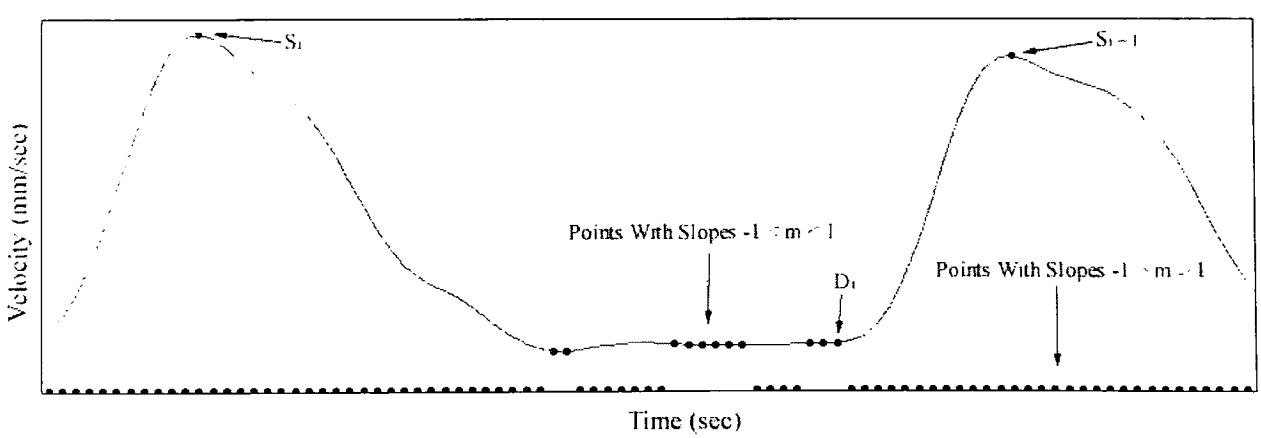

Figure 2.3 Plot describing the search criteria for the end-diastolic velocity (D). The points represented by (•) indicate where in the fetal record the data has point-wise slopes (m) in the range of $-1 < m < 1$ or $-1 > m > 1$.

derivative is calculated and only the concave-up data region preserves its velocity value. And all other data that does not meet both the slope and curvature criteria are reset to zero as indicated by (•) in Figure 2.3. The final step in the end-diastolic pulse-velocity determination is to perform a backward search from S_{i+1} to S_i locating the first non-zero value, which is taken as the end-diastolic velocity (D_i) between these respective pulse-velocities (see Figure 2.3).

The mean pulse-velocity (M) can then be calculated by averaging all the values between two consecutive end-diastolic points. Once the three essential pulse-velocity landmark values S, D, M, and their respective temporal location within the data record are found, the pulse velocity waveform indices can be calculated as described in Section 2.2.

2.1.2 Average Pulse-Velocity Waveform Definition

As noted above, the PVD algorithm has the ability to decompose a pulse-velocity time series into a pulse-velocity train. Here each pulse-velocity can be scrutinized in order to determine pulse parameters S, D, and M and the pulse indicies noted in Section 2.2. Since a given fetal velocity record may be composed of several dozen consecutive pulse-velocities (Figure 2.4), statistical analysis of the pulse-derived indices would be necessary to yield a "fetal-average" value for the respective indices such that fetal-to-fetal comparisons may be subsequently performed.

A different approach to analysis is to extract each individual cardiac cycle and average pulse-velocity points in the extracted data to compile an average cardiac cycle that is characteristic of the entire fetal pulse-velocity wavetrain (Figure 2.4).

For example the first point in each pulse is averaged with the first point in the second pulse and so on until all the points are averaged for each cycle. Hence the entire family of pulses (Figure 2.4) for a given fetus would be condensed to a single representative "average pulse-velocity" of the entire fetal velocity record (Figure 2.5).

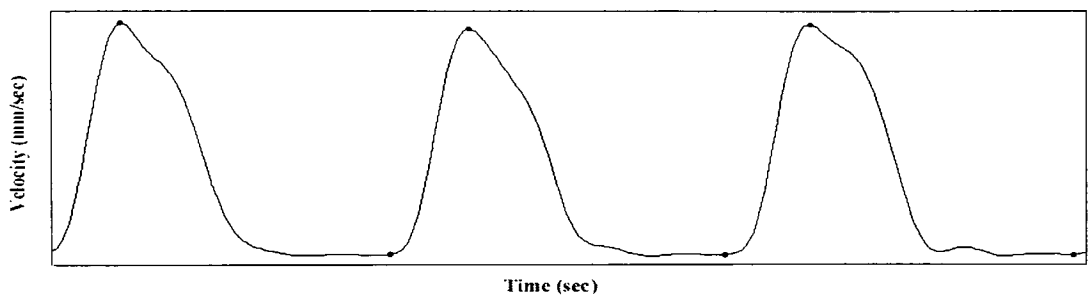

Figure 2.4 Plot of multiple consecutive velocity pulses.

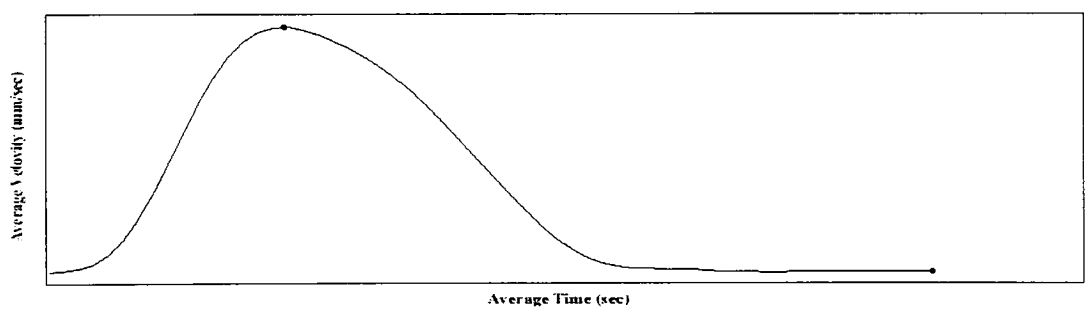

Figure 2.5 Plot of an averaged pulse-velocity calculated from multiple velocity pulses.

This allows all the information contained in a pulse-velocity wave train to be represented by one average pulse-velocity. The PVD algorithm may then determine the average pulse-velocity parameters S, D, and M for use in comparing fetal representative velocity waveform indices. Likewise the average pulse-velocity may be used *in toto* for comparison between fetuses (to be discussed below). Note that individual pulse-velocities may not be of equal temporal duration (i.e. unequal number of pulse-velocity data points) due to the variable nature of fetal heart rate. Hence, when computing the average pulse-velocity, individual pulse velocity waveforms were truncated in duration to

equal the shortest duration pulse-velocity. The truncation occurred at the tail-end of phase 3 (Figure 2.2) in all cases so as to affect an individual velocity pulse only within the (relatively) non-varying region just prior to end-diastole.

2.1.3 Evaluation

Part of the PVD algorithm is to determine (section 2.2) and write the values of the PI, RI, the AB ratio, and the diastolic decay constant (τ) to a text file, so as to allow other programs such as MATLAB and Excel to read these data files for subsequent analysis. Excel (Microsoft Corp., Redmond WA) was used to produce multiple plots for data comparison. While the MATLAB (The Mathworks, Inc., Natick MA) neural network algorithms were employed to investigate whether fetal gestational age discrimination could be conducted using pulse-velocity waveforms indices.

2.2 Velocity Waveform Characteristics

2.2.1 Index Definition

For the purpose of this study it was necessary to determine velocity waveform indices, such as the pulsitility index (PI), the resistance index (RI), the AB ratio, and the diastolic decay constant (τ). As a first step in the calculation of the pulsatile waveform indices, the end-diastolic velocity (D), peak-systolic velocity (S), and mean pulse-velocity (M) were determined within each velocity pulse (see Figure 2.6). This determination scheme was detailed previously in Section 2.1.

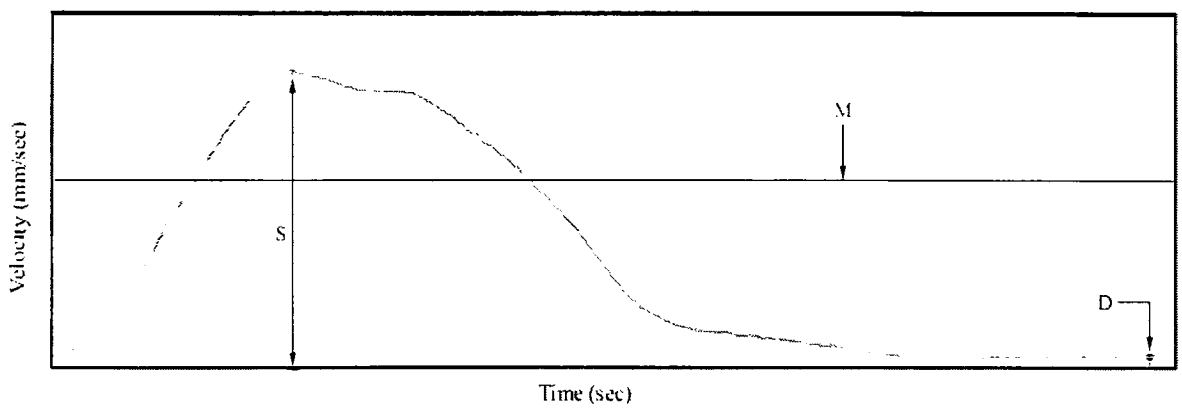

Figure 2.6 Plot of a single cardiac cycle pulse-velocity waveform.

Historically the pulsitility index was first calculated using the Fourier transform of the Doppler blood velocity pulse waveform (Evans *et al*, 1989), where:

$$PI = \sum_{n=1}^{\infty}\left(\frac{a_n^2}{M^2}\right) \qquad \begin{array}{l} a_n = Amplitude\ of\ the\ n^{th}\ harmonic \\ M = Mean\ height\ of\ an\ individule\ cycle \end{array} \qquad \text{Eqn. 2.1}$$

But this method was deemed by early researchers to be too tedious and time consuming due to the slow speed of early computers. Hence a simplified method for computing PI was introduced such that

$$PI = \frac{S - D}{M}$$

S = *Systolic amplitude*
D = *Diastolic amplitude*
M = *Mean height of individule cycle*

Eqn. 2.2

Likewise, Porcelot's resistance index is defined as (Evans *et al*, 1989):

$$RI = \frac{S - D}{S}$$

S = *Systolic amplitude*
D = *Diastolic amplitude*

Eqn. 2.3

Scrutiny of Equation 2.2 and Figure 2.6 reveals that an individual Doppler velocity waveform may possess various values for S, D, and, M which render no theoretical upper limit to the pulsitility index (PI); although, clinical usage of Equation 2.2 has shown non-infinite upper limits in practice, which are typically between .5 and 1.5. Likewise, Equation 2.3 would suggest a theoretical range for the RI between 0 and 1. The normal range for the resistance index is $0.72 < RI < 0.85$, for late gestation fetuses (Thompson *et al*, 1986). Values of the RI which exceed 0.85, which signify low blood flow, are indicative of a vascular obstruction, while RI values below 0.72 typically represent higher than normal blood flows (Thompson *et al*, 1985).

The fourth most common Doppler velocity waveform characteristic index is the AB ratio (Equation 2.4).

$$AB = \frac{S}{D}$$

S = *Systolic amplitude*
D = *Diastolic amplitude*

Eqn. 2.4

The diastolic decay constant (τ) is used in the current study to represent the best exponential fit of the data between peak-systole (S) and end-diastole (D).

$$\tau = \frac{\ln F/a}{X}$$

τ = *Decay Constant*
F = *Output of the Best Exponential Fit*
X = *Input Array of Velocities Between S and D*
a = *Amplitude*

Eqn. 2.5

The diastolic decay constant can be postulated based on an assumed relationship between blood flow and an R-C-R circuit model of the placental circulation in cardiovascular physiology, also known as a "Windkessel Model". The Windkessel model is an electrical circuit that represents the distal and proximal vascular resistance, and the capacitance of the blood vessels (Figure 2.7).

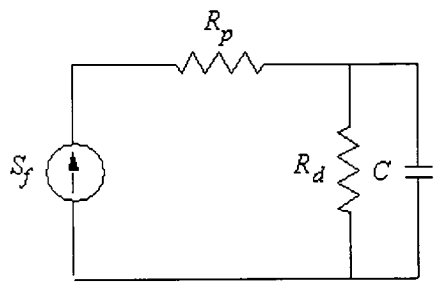

R_p = Lumped Resistance of Proximal arteries
R_d = Lumped Resistance of Distal arteries
C = Lumped Elastance of the Blood Vessels
S_f = Source of Flow

Figure 2.7 The Three Element Windkessel Model.

Using Kirchhoff's current and voltage laws, the decay constant (τ) as used in Equation 2.5 can be related to the Windkessel model parameters (Kalegaonkar, 1998).

$$\tau = \frac{R_p + R_d}{CR_pR_d} \qquad \text{Eqn. 2.6}$$

R_p = Lumped Resistance of Proximal arteries
R_d = Lumped Resistance of Distal arteries
C = Lumped Elastance of the Blood Vessels

The Doppler velocity waveform indices used herein are directly dependent on impedance of the placental vascular network, heart rate, and gestational age (Ursem *et al*, 1998). Because the waveform indices are susceptible to changes in gestational age and impedance they are likely candidates for ascertaining the age and health of a fetus (Thompson *et al*, 1985).

2.3 Neural Network Discrimination

2.3.1 Neural Network Background

Artificial neural networks (ANN) are architecturally and functionally based on the interconnections found in biological central nervous systems (CNS). The massive connections (10^{11}) in the human CNS allow for the ability to store and synthesize massive amounts of information that can be recalled instantly for any number of purposes. For example, during reading the brain recognizes and associates each letter and combinations of letters to sounds (phonics) or combinations of sounds (words). In sound recognition the brain can, with appropriate training, determine whether a sound is emanating from a known source and determines likely sound generation sources without visualization. The principles of recognition can also be applied to judgment making abilities. For example, appropriately trained (or experienced) health care professionals may diagnose certain heart pathologies utilizing only the sound of the beating heart, monitored through a stethoscope.

An artificial neural network attempts to simulate the functionality of the brain, wherein it is possible to store data within the network for use later in decision-making processes. A neural network algorithm structurally consists of parallel neurons similar to biological nerve cells in the CNS (Figures 2.9 and 2.10).

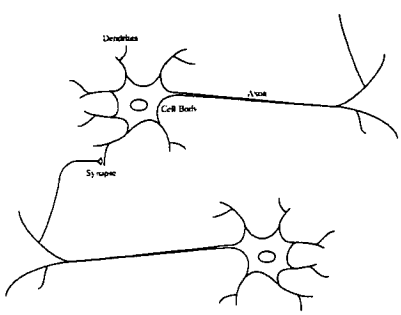

Figure 2.9 Image of biological neurons. (Adapted from Hagen *et al.*)

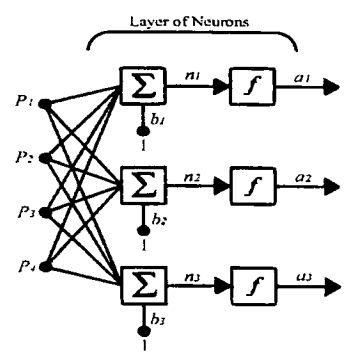

Figure 2.10 Image of an artificial neural network. (Adapted from Hagen *et al.*)

Figures 2.9 and 2.10 indicate that the neural network structure shares and stores information with other paralleled neurons from an input of data (or stimulus as in the case of the biological neuron). In addition to the architectural similarity between the biological neural networks (Figure 2.9) and artificial neural networks (Figure 2.10), there is a functional similarity as well. One of the functions of the nerve cells is determining the significance of inputs via stored sensitivities associated with specific stimuli. So, when the neuron encounters a stimulus that is important, or critical to remember, it weighs the stimulus more than other stimuli that are being received at the same time. Hence the neuron puts more emphasis (weight) on the more important input, relative to the less significant input. Similarly an artificial neural network also applies weighting to the various neuron inputs that contain important information.

Artificial neural networks (ANN) utilize training of neurons in order to instill decision-making (classification) abilities. Training a network involves use of the "feature vector" with a set of corresponding "target vectors". Here a feature vector will contain all the information a neural network needs to perform the appropriate training (for example a typical feature vector may contain the PI, RI, AB ratio, and τ). Target vectors are typically integer values, which correspond to a classification, that are used to evaluate the output of the neural network. When the input data and target vectors are entered into the ANN, training must be performed to adjust the weights and biases in a systematic manner such that the network output values are close to the target vector values using a summed squared error criterion. At the end of training an unclassified set of data (feature vector) can then be entered into the trained neural network for classification analysis.

2.3.2 Network Training and Evaluation

A neural network may be used to discriminate between data categories provided that an appropriate set of network weights and biases are calculated *a priori*. Hence, weights and biases are the quantities determined during network training. Weights (W) are placed on the inputs to the neurons, which are adjusted according to the numerical significance or importance of the input. For example, a single neuron with multiple inputs is depicted in Figure 2.11, which shows the process from the input of the feature vector (R) to the output (a_1). Where (b_1) is the neuron bias input.

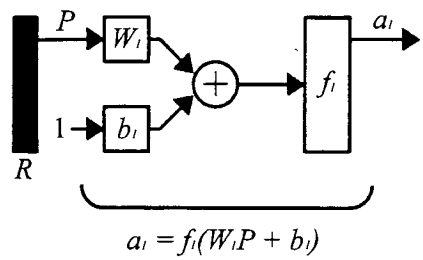

Figure 2.11 Model of a single layer neuron with an input array of values. (Adapted from Hagen *et al.*)

As this network trains the weighting (W) will increase if the network puts more emphasis on a specific input (P). If the network output (a) is less sensitive to the input (P), its corresponding weight (W) will decrease accordingly. Selection of the bias value (b) is similar to that of the weights except the bias input is always 1. The bias value is also subject to modification during network training.

"Learning" is the process by which the weights and biases are adjusted to attain a desired network behavior. With non-linear data, the learning rule most often used to train is backpropagation (Hagen *et al*, 1996). An important part of backpropagation is the performance index, which focuses on the calculation of the sum of the mean square error (SSE), where:

$$SSE = \sum (T - a)^2 \,. \qquad \text{Eqn. 2.7}$$

T = Target Vector for a Given Input (Training) Vector
a = Network Output Vector for a Given Input (Training) Vector

As the training begins, the input training data are entered with the corresponding target vectors. The training data provides the network with an array of specimen data that exemplify the characteristics of desired network classification.

Each evaluation of the network is termed an "epoch", where the output of the network is compared to the target vector. The neural network is then "fine-tuned" by adjusting the weights and biases in order to minimize the SSE to a user defined error goal. Training is complete when the error goal has been reached. Automated adjustment the weights and biases maybe calculated using Equations 2.8 and 2.9.

$$W^m_{i,j}(k+1) = W^m_{i,j}(k) - \alpha \frac{\partial \hat{F}}{\partial W^m_{i,j}} \qquad \text{Eqn. 2.8}$$

$$b^m_i(k+1) = b^m_i(k) - \alpha \frac{\partial \hat{F}}{\partial b^m_i} \qquad \text{Eqn. 2.9}$$

α = *Learning rate*
$W^m_{i,j}$ = *Weight of the* m^{th} *layer,* i^{th} *element of the row,* j^{th} *element of the column*
b_i = *Bias*
$\hat{F}$ = *SSE*

Here, the learning rate (α) can be adjusted during the training of the network. The modification of α is dependent on the SSE and will be discussed in detail below. To calculate network weights and biases (Equations 2.8 and 2.9, respectively) the partial derivative of $\hat{F}$ needs to be computed. With networks of multiple layers (see Figure 2.12) the SSE is an indirect function of the hidden layers, thus the partial derivative is not an explicit function of the weights and biases in the hidden layers. So, the easiest way to calculate the derivative is to use the chain rule expansion as described in detail by Hagen *et al* (1996).

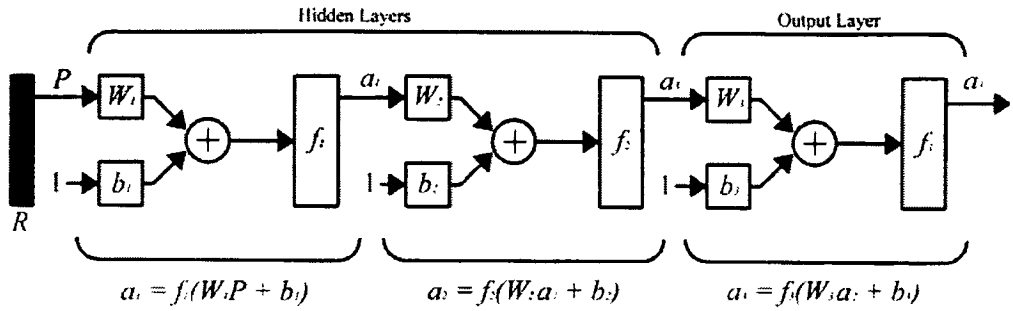

Figure 2.12 Model of a multiple layer network with an input array of values. (Adapted from Hagen et al.)

To improve the performance of the network, heuristic modifications are added in the backpropagation training method. The convergence of the SSE goal can be improved by smoothing oscillations in a trajectory utilizing the so-called "momentum function", which is in essence a low pass filter. Basically the momentum modification allows neural network training the ability to track the average value of the data entered but with much less oscillation. The filtering performed by the momentum helps network training avoid getting caught in a shallow minimum (Figures 2.13 and 2.14).

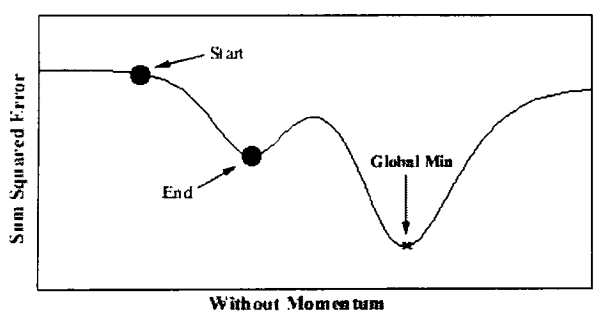

Figure 2.13 Illustration of a neural network without momentum.

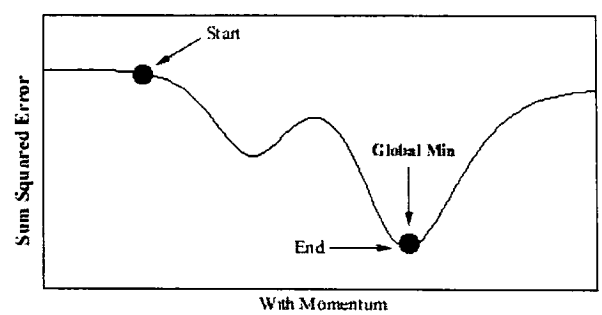

Figure 2.14 Illustration of a neural network with momentum.

Another modification involved with a speedier convergence is the adjustment of the learning rate (α). The learning rate is allowed to increase when SSE gradients are "flat", while the learning rate is decreased when SSE gradients are substantially non-zero.

Adjustments to the learning rate are made according to three rules of performance on a backpropagation network (Hagan et al 1996):

1) If the squared error (over the entire training set) increases by more than some set percentage ζ (typically one to five percent) after a weight update, then the weight update is discarded, the learning rate is multiplied by some factor $0 < \rho < 1$, and the momentum coefficient γ (if it is used) is set to zero.

2) If the squared error decreases after a weight update, then the weight update is accepted and the learning rate is multiplied by some factor $\eta > 1$. If γ has been previously set to zero, it is reset to its original value.

3) If the squared error increases by less than ζ, then the weight update is accepted but the learning rate and momentum coefficient are unchanged.

Where:

γ = Momentum Coefficient
ζ = Percent Increase in the Summed Square Error Over the Entire Training Set
ρ = Learning Increment
η = Learning Decrement

and (Demuth and Beale, 1994):

Learning Rate – A training parameter that controls the size of the weights and bias, changes during learning.
Learning Decrement – The multiplier used to decrease an adaptive learning rate.
Learning Increment – The multiplier used to increase an adaptive learning rate.
Momentum – A technique often used to make it less likely for backpropagation network to caught in a shallow minima.

By utilizing these rules the adjustment of the learning rate at the appropriate epoch, can be automated to "optimize" the speed of convergence of network training. Optimization of these parameters is a trial and error procedure. This is because various sets of data give different convergence rates, relating to the nature of the data. So any results from modifications of these parameters are only applicable to the data collected for this research.

2.3.3 Experimental Data Segregation

The current investigation consists of two experimental groups: the training set and the testing set. Both data groups are collected from several dozen patient observations at 10, 11, 12, and 13 weeks of gestation. All observations were made with maternal informed consent, and conducted with ethics committee approval from all institutions participating in this study. Each patient file is analyzed using the PVD program and using the maximum frequency reconstruction method (Gallagher, 1995; Kempski *et al*, in review, and Ursem *et al*, 1998) resulting in a list of values consisting of various Doppler velocity waveform indices (the PI, RI, the AB ratio, and τ) from each cardiac cycle in the velocity waveform. Respective pulse-velocity indices were averaged across the fetal data record so that fetal average indices were obtained.

Depending on the number of patient files in each gestational week, a maximum of five randomly selected fetal data records were used as testing files for the neural network, with the remaining fetal records at a given gestational week were used to create network training vectors. Ideally after neural network training, robust discrimination should be possible between fetal index (feature vector) data obtained at weeks 10, 11, 12, or 13 weeks of gestation.

To determine if the diastolic decay constant (τ) was an accurate measure of the cardiac cycle timing, the mean square error (MSE) is calculated for the averaged pulse velocity waveform data (see Figure 2.15) between $\overline{S}$ and $\overline{D}$ compared to the best fit curve defined by Equation 2.5.

Eqn. 2.10

n = Number of Elements in the Input Sequence
f(I) = Best Exponential Fit to Velocity Segment Between $\overline{S}$ *and* $\overline{D}$
y(I) = Actual Velocity Segment Between $\overline{S}$ *and* $\overline{D}$

$$MSE = \left(\frac{1}{n}\right)\left(\sum\left(f(i) - y(i)\right)^2\right)$$

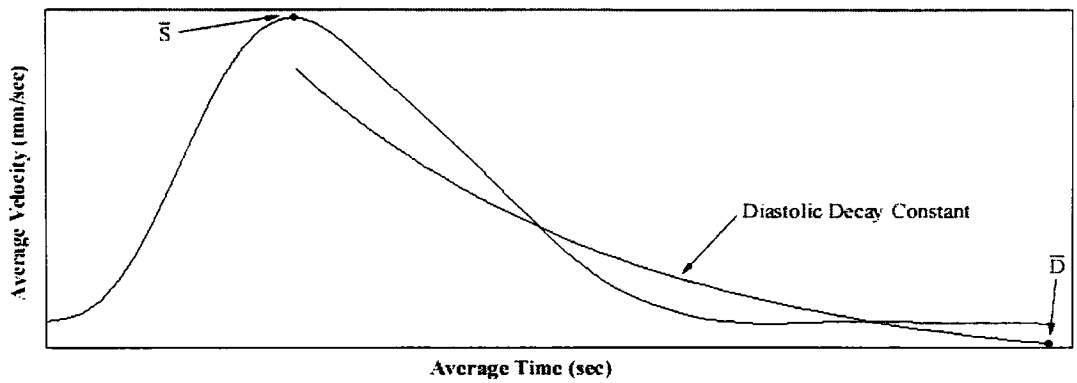

Figure 2.15 Visual comparison between the exponential best fit curve and an averaged pulse-velocity.

Likewise, fetal velocity waveform indicies may be plotted versus each other to observe whether data "clustering" was evident (Figure 2.16). Such clustering may be indicative of self-segragation between fetal gestational age groups and is known to be desirable from a classification perspective (Duda and Hart, 1973).

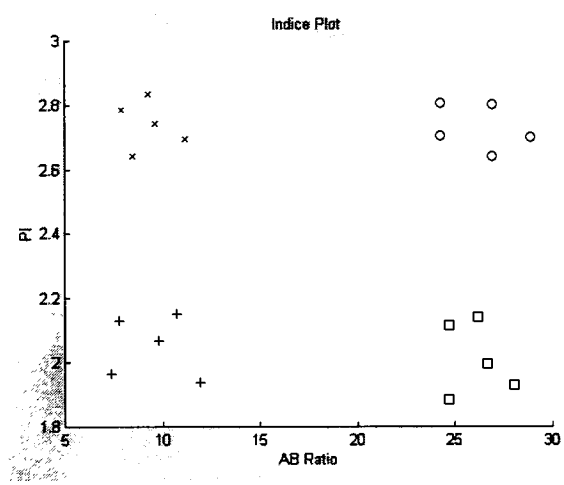

Figure 2.16 Hypothetical example of velocity wave form index data "clustering".

2.3.4 Network Construction

Nominally the network was configured as a two-layer system, using MATLAB v4.2c (The Mathworks Inc., Natick MA) with the neural network TOOLBOX v2.0b.1 (see appendix A for the MATLAB scripts). The hidden layer (layer 1) contained six neurons with three inputs, while the output layer (layer 2) contained two neurons (Figure 2.16).

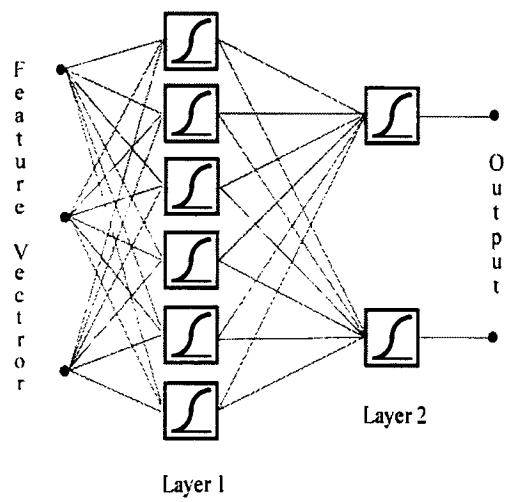

Figure 2.16 Model of a multiple layer, multiple input, multiple neuron backpropagation network.

All the layers utilized non-liner transfer functions, specifically the log-sigmoid transfer function (Equation 2.11).

$$a = \frac{1}{1 + e^{-n}} \qquad \begin{array}{l} n = Input \\ a = Output \end{array} \qquad \text{Eqn. 2.11}$$

Represents a log sigmoid transfer function.

The input feature vector was first created to contain the respective fetal averaged velocity waveform indices. The gestational week categories are identified by the two output

neurons with assigned target vectors such that "ideal" neuron outputs are given by [$a_{2,1}$, $a_{2,2}$], where the assigned target vectors for week 10 are [0,0], week 11 are [0,1], week 12 are [1,0], and week 13 for [1,1].

Alternatively, the network input "feature vector" could be the average pulse-velocity data values. Hence, the network training and testing could occur by use of an entire average pulse-velocity data series as opposed to the "reduced" set of fetal averaged velocity waveform indices noted above.

In the analysis results which follow, both feature vector approaches were evaluated to assess whether fetal age discrimination between 10 to 13 weeks gestation is possible.

Chapter 3 Results

3.1 Diastolic Decay Constant

Figure 3.1 depicts a "typical" superposition of fetal average pulse-velocity waveform and the "best-fit" exponential decay curve defined by Equation 2.5. Computation of the MSE between the "best-fit" curve and the diastolic portion of this average pulse velocity waveform was 268.2.

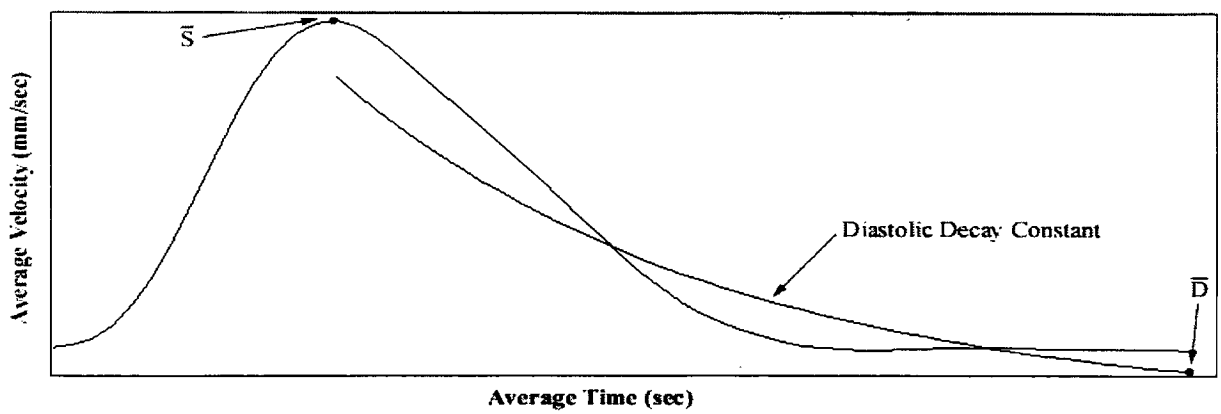

Figure 3.1 Visual comparison between the exponential best fit and an averaged cardiac cycle.

As depicted in Figure 3.1, this "best-fit" approximates the shape of the average pulse-velocity trace after peak systole. However the rate of diastolic decay of the average pulse-velocity waveform is more severe than that defined by an exponential decay. This poor fit was consistently observed for all data files processed during the current study. As such, the diastolic decay index, τ, was not used as an element in the waveform index feature vectors employed for neural network training or classification.

3.2 Velocity Waveform Index Training and Classification

Neural network training was first attempted using feature vectors defined using the PI, RI, and AB ratio fetal velocity waveform indices. This process was guided, in part, by the work of Morrow (1998) which indicated that a two-layer back propagation network was sufficient to classify changes in gestational age measured over trimesters. However, network training for fetuses with gestational age of 10, 11, 12, or 13 weeks proved problematic, plagued by slow convergence.

Initially the slow convergence of network training was thought to be a consequence of the initial conditions of the heuristic modifications (the learning rate, learning increment, learning decrement, and momentum). After many attempts (to no avail) using, heuristic parameters of various bounds, adjustments of the size of the neural network were conducted. Network configurations ranged from two layer networks with six neurons in layer one and two neurons on the output layer as described in Section 2.3.4, to a three layer network with 12 neurons in layer one, 32 neurons in layer two, and two neurons in the output layer. Using several combinations of the heuristic modifications in conjunction with different network configurations, it became evident that the network could not train with the given velocity waveform index data. For each configuration the network was unable to converge to the proper error goal (SSE < .02) after more than $4e^5$ epochs. According to Morrow (1998) the network should be able to converge to the error goal within 7000 epochs. After further scrutiny this lack of convergence of the SSE was attributed to an overlap in hemodynamic indices for fetuses in the study group.

Figure 3.2 through 3.4 indicate that, for the data used in this study, there was not a consistent clustering of hemodynamic index values associated with gestational age. Such cross-pollination between age groups is shown explicitly in Figures 3.2, 3.3, and 3.4 using the average waveform indices for each fetus (See Appendix B). Since these pulse-velocity waveform indices are not "clustered", the neural network cannot be effectively trained so that the weights and biases can discriminate the target age groups. Without effective network training, use of the neural network and pulse-velocity waveform indices for gestational age discrimination was not possible.

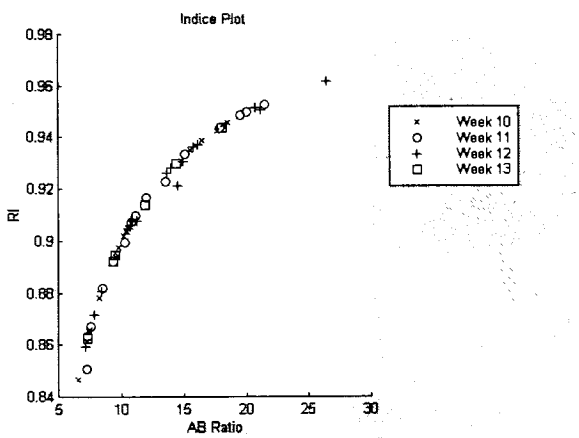

Figure 3.2

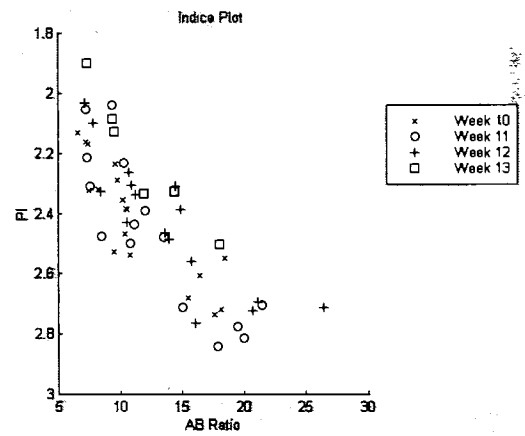

Figure 3.3

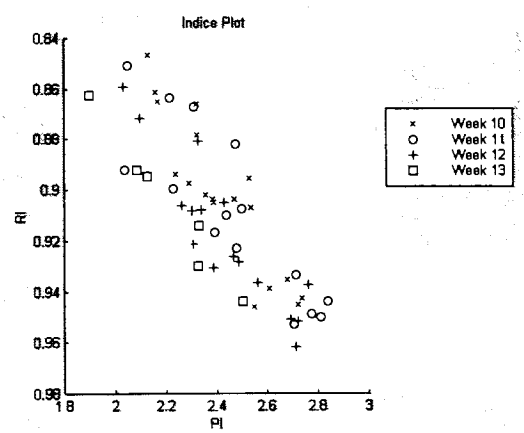

Figure 3.4

Figures 3.1, 3.2, 3.3 Graphical depiction of fetal blood pulse-velocity indicial "signatures". Plots show a lack of segregation by age when individual fetal PI, RI, and AB ratio indices are employed to classify gestational weeks 10, 11, 12, and 13.

Instead of using the average pulse-velocity waveform indices extracted from each fetal record for training, the data was "compressed" by further averaging across a given gestational week. Hence gestational "weekly-average" PI, RI, and AB ratio values were computed and provided four feature vectors (see Appendix B), each representing the respective gestational week 10, 11, 12, and 13 index data. Figure 3.8 is the analysis result of testing feature vectors that spanned 10 – 13 weeks of gestation. The results indicated in Figure 3.5 show that the artificial neural network testing, following training with weekly-average feature vectors containing waveform index information, indicates that the classification capabilities of the testing vectors is not robust.

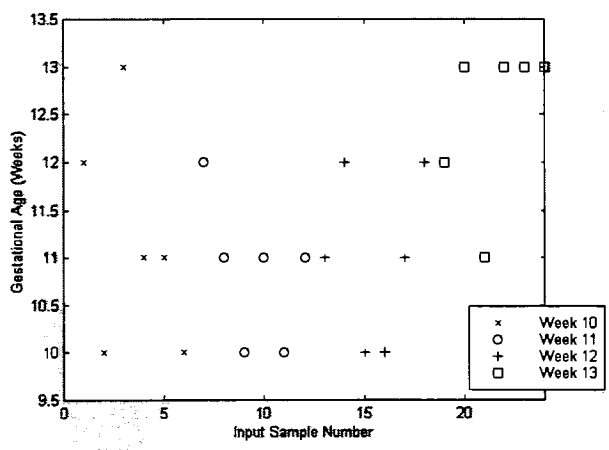

Figure 3.5 The test feature vectors are from known gestational age classifications as indicated in the figure legend. The highest sample number in any group represents the weekly-average training vector for that group, which was fed-back into the network as a self-consistency check.

Patient Number	Sample Number	Fetus Age	Day	PI	RI	AB	τ
A02_0019UA1	1	Week 10	0	2.6054	0.9391	16.4267	37.8985
A10_0129UA1	2		3	2.4698	0.9035	10.3942	34.9247
A18_0256UA1	3		3	2.2375	0.8937	9.5739	32.3336
A22_0311UA1	4		3	2.3577	0.9019	10.2075	32.1922
A03_0025UA2	5		4	2.1319	0.8467	6.5778	25.5024
Avg Training Vector	6		Test	2.4319	0.9020	11.5572	33.3533
A05_0059UA1	7	Week 11	4	2.8132	0.95	20.0129	39.5927
A08_0107UA1	8		6	2.4742	0.8818	8.4733	32.2863
A09_0119UA2	9		4	2.4997	0.9072	10.7903	35.6923
A18_0254UA1B	10		2	2.4806	0.9229	13.5081	35.6319
A18_0254UA1NB	11		2	2.4383	0.9098	11.1538	33.9196
Avg Training Vector	12		Test	2.4532	0.9095	13.0386	33.9183
A03_0031UA3	13	Week 12	0	2.7639	0.9375	16.0565	40.3843
A04_0040UA1	14		0	2.7129	0.9619	26.4187	43.5124
A04_0052UA1	15		6	2.3399	0.9076	11.2024	34.1108
A17_0241UA1	16		2	2.431	0.9048	10.5465	28.2708
A08_0103UA1	17		2	2.0326	0.8594	7.1359	31.2273
Avg Training Vector	18		Test	2.4012	0.9159	12.9994	32.4944
A18_0258UA1	19	Week 13	5	2.3268	0.9299	14.3757	29.2068
A16_0230UA1	20		5	1.8988	0.8626	7.325	26.6326
A14_0195UA1	21		0	2.3337	0.9138	11.9449	36.2882
A11_140UA1	22		4	2.1261	0.8945	9.5643	33.2097
A05_0069UA1	23		?	2.0867	0.8923	9.3779	28.8966
Avg Training Vector	24		Test	2.3518	0.9152	13.5062	29.8955

Table 3.1 Chart of the fetal records used to test the neural network.

3.3 Average Pulse Velocity Training and Classification

Another approach to network training employed the average pulse-velocity waveform data as the input feature vector, instead of the waveform indices. Figure 3.6 depicts all 73 fetal average pulse velocity waveforms plotted for comparison purposes.

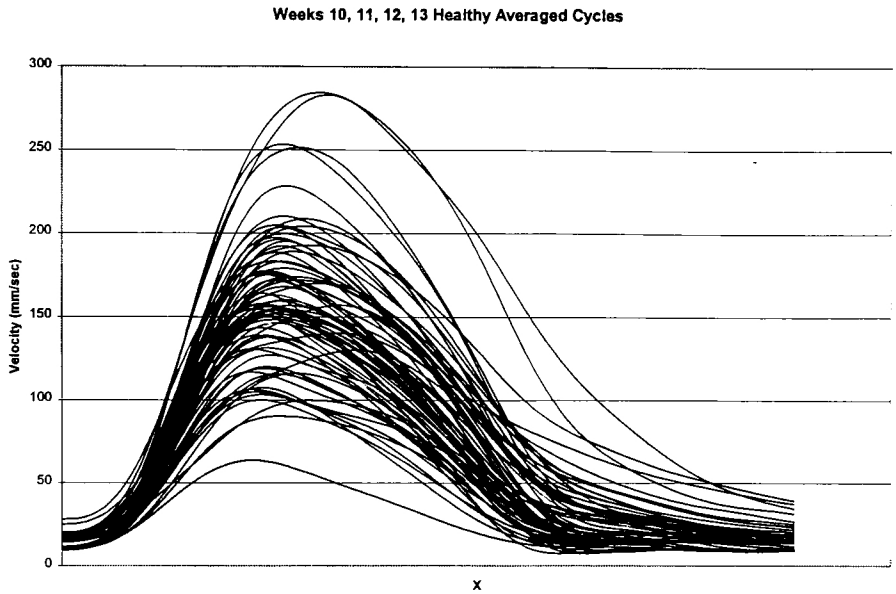

Figure 3.6 Plot of 73 averaged cardiac cycles. Ranging from 10 to 13 weeks of gestation

Visual assessment of Figure 3.6 suggests that clustering by gestational age maybe problematic (see Appendix C for a separate comparison by gestational week). These average pulse-velocity data were further condensed to single (mean) average pulse-velocity waveforms per gestational week via averaging all fetal waveforms within a given gestational week. These weekly average pulse-velocity data are shown in Figure 3.7. Modest segregation between gestational age groups is evident in Figure 3.7, suggesting that neural network training may be possible if the weekly average pulse-velocity data are used for training purposes. By assigning a target vector to each week of gestation (week 10 [0,0], week 11 [0,1], week 12 [1,0] and, week 13 [1,1]) the neural network was able to distinguish between the

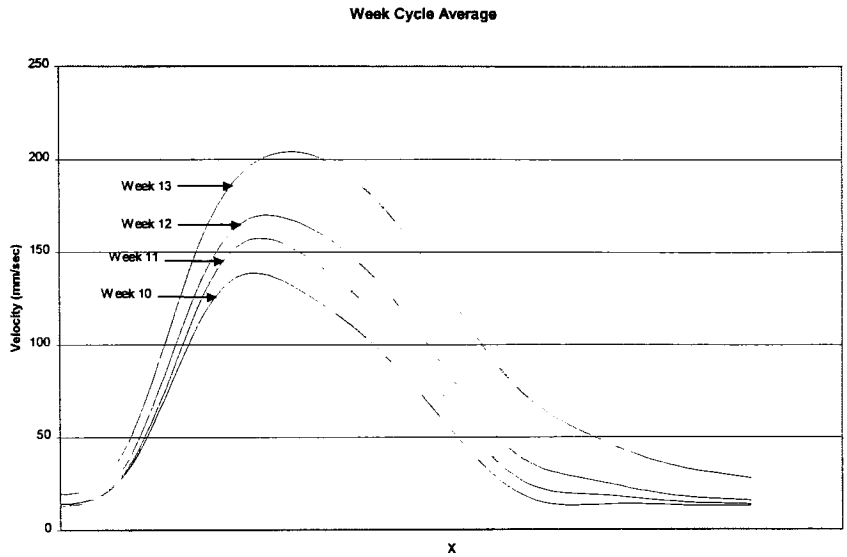

Figure 3.7 Graphical depiction of fetal pulse-velocity waveform "signatures" following weekly-averaging. Ordinate is velocity in mm/sec, abscissa (X) represents time. Plots show that segregation by gestational week may be possible due to differences in waveform shape and/or magnitude

data shown in Figure 3.7. Thus, a set of weights and biases were found which were applied to assess the classification of the testing vectors using average pulse-velocity records from the same fetuses noted in Table 3.1. The weights and biases calculated by the neural network using the weekly average pulse-velocity data were then used to evaluate the fetal average pulse-velocity waveform data set-aside for testing purposes (see Table 3.1). Of the five individual (fetus) feature vectors per gestational age group, Figure 3.8 shows that successful classification occurred in four of five (4/5) trials for week 10, three of five (3/5) trials for week 11, two of five (2/5) trials for week 12, but only one of five (1/5) trials at week 13. Note that unsuccessful classifications shown in Figure 3.8 may be the result of the individual embryo waveform overlaps between age

groups. Examining Figure 3.8 it can be seen that the neural network was not able to classify all the individual fetal average pulse-velocity waveform

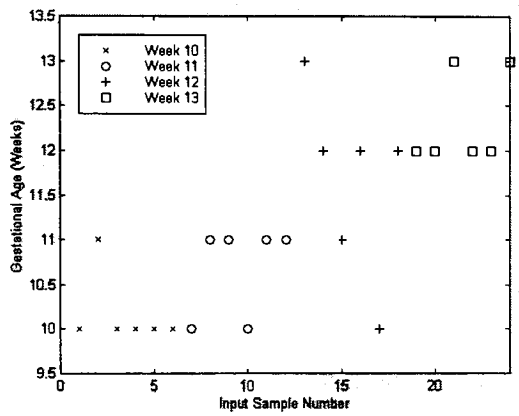

Figure 3.8 Artificial neural network testing following training with weekly-average feature vectors containing pulse-velocity waveform data. The test feature vectors are from known gestational age classifications as indicated in the figure legend. The highest sample number in any group represents the weekly –average training vector for that group, which was fed-back into the network as a self-consistency check. Perfect classification would result in a sequence of "steps". The network passes the self-consistency check and classification, while not perfect, is more robust than that previously conducted using index-based feature vectors.

data into the correct gestational age groups. These results stem from the fetal average pulse-velocity overlap shown in Figure 3.6. Calculating the confidence interval at a 95% confidence level (see Figure 3.9) provides a graphical interpretation of the error found in Figure 3.8. The comparison plot indicates that there is significant overlap in confidence intervals between consecutive weeks 11 and 12 of gestation to the point where proper discriminatory ability failed (additional confidence interval plots are shown in Appendix D).

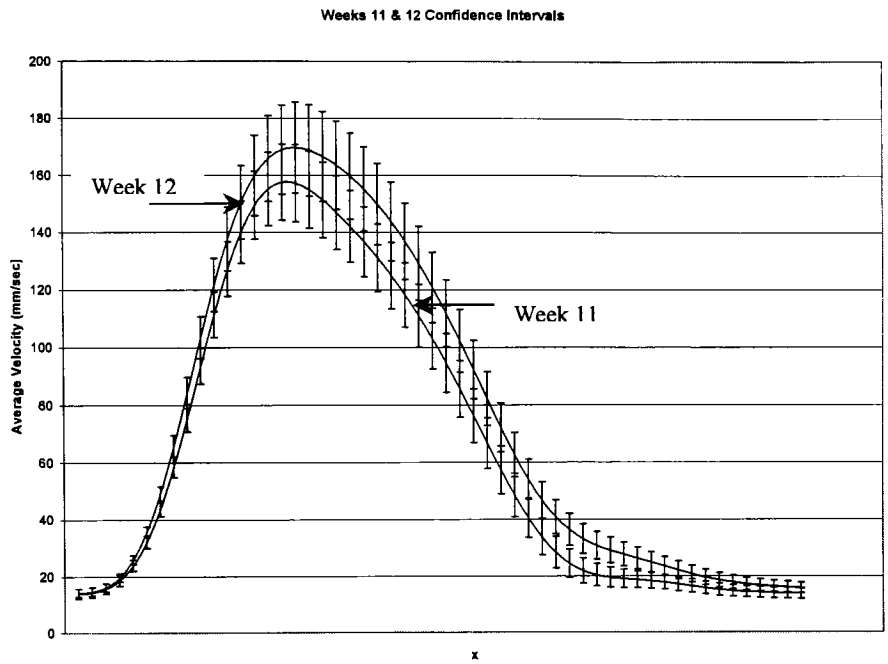

Figure 3.9 Graphical comparison of averaged fetal pulse-velocity waveforms of gestational weeks 11 and 12 with corresponding confidence intervals (calculated with a 95% confidence level).

While the weekly average pulse-velocity training vectors depicted in Figure 3.7 show modest segregation, the average pulse-velocity testing vectors used (other than the fed-back weekly average pulse-velocity vectors) for evaluation appear to posses a substantive variance based on the results depicted in Figure 3.8. This is likely due to overlap between individual average fetal pulse-velocity data series across gestational age groups (see Appendix C). Hence, misclassification ensues. Figures 3.5 and 3.8, show that Doppler waveform indices afford a decreased ability to differentiate between gestational weeks when compared to classification attempts using average pulse-velocity waveform data.

Chapter 4 Discussion

4.1 Diastolic Decay Constant

The diastolic decay constant was determined to not have an efficient correlation to the average pulse-velocity. Significant error was observed due to the steep run off after peak-systole ($\bar{S}$, Figure 3.1). The error was largely due to the steep decline in velocity time series value after peak systole ($\bar{S}$), which the simple exponential function was unable to mimic. As such, a more elaborate functional definition is required to appropriately model the average pulse-velocity waveform over the period from peak-systole ($\bar{S}$) to end-diastolic velocity ($\bar{D}$) values. Furthermore, the diastolic decay constant τ was not employed during subsequent neural network analysis of fetal hemodynamic index data.

4.2 Waveform Indices and Classification

As development of the fetal circulatory system progresses, blood flow velocity also changes. Throughout the last 20 weeks of development, characteristic pulse-velocity waveform indices become differentiable at various gestational ages and health condition (Thompson and Trudinger, 1989). However, between the gestational ages of 10 to 13 weeks, the current study has discovered that pulse-velocity waveform characteristic indices are not the best approach for fetal health assessment, since variations in fetal data cannot be consistently classified into their appropriate gestational week (see Figure 3.6). This lack of classification ability stems from the overlap observed in the fetal waveform

velocity indices for the gestational ages used for this study. Such overlap is explicitly seen in Figures 3.2 to 3.4.

According to Wright et al, (1997), neural network testing is possible for fetal pulse-velocity waveforms between 17 to 20 weeks of gestation. Using late second trimester Doppler waveforms a success rate of 100% classification with the carotid artery, and 94% classification with the femoral and popliteal artery has been achieved (Wright et al., 1997). Thus the fetal gestational week 10, 11, 12, and 13 pulse-velocity waveforms used in the current study may not be distinct enough to be successfully differentiated when using the PI, RI, and, AB ratio indices. Indeed, even use of the average pulse-velocity waveform index data did not afford a robust fetal age discrimination based on the results of the current study.

Figures 3.2, 3.3, and 3.4 show that there was no evident clustering of the average fetal indices according to gestational age between 10 to13 weeks. Therefore since grouping according to gestational age was not apparent, the neural network was unable to separate the indices for classification purposes.

Section 4.3 Average Pulse Velocity and Classification

The current study suggests that use of pulse-velocity waveform data as the "feature vector" used in classification has modest discrimination capability, although misclassifications occur as seen in Figure 3.8. Hence, more patient observations (i.e. more data records) may be required if robust classification is to be achieved. Data depicted in Appendix C show large amounts of overlap in fetal average pulse-velocity waveforms from 10 to 13 weeks gestation. This waveform overlap suggests that

individual patient waveform data possess considerable variance which renders discrimination difficult unless many patients are averaged together to lessen the variance.

Chapter 5 Conclusion

Examination of the Doppler velocity waveform indices has shown that during early gestation (weeks 10 to 13) the PI, RI, and AB ratio are not powerful classification indices based on the data used for this study. Analysis using the average pulse-velocity waveform resulted in better classification outcomes, however robust discrimination was not achieved.

That the Doppler velocity waveform indices appear to be a much less reliable assessment method than the average pulse-velocity waveform suggests that the calculation of the PI, RI, and AB ratio omit valuable classification information. The lack of consistent classification utilizing pulse-velocity waveform time series information suggests that, at these early gestational ages, large numbers of patient observations ($n > 20$) may be required to train robust neural network classification algorithms. Based on the limited data used for this study, neither characteristic indices nor pulse-velocity waveform time series data provide reliable fetal age discrimination amongst healthy maternal-fetal pairs.

References

Clark, E.B., 1986, "Cardiac Embryology: Its Relevance to Congenital Heart Disease", *American Journal of Diseases of Children*. Vol. 140 pp. 41-44.

Clark, E.B., Takao, A., 1990, "Overview: A Focus for Research in Cardiovascular Development", *Developmental Cardiology: Morphogenesis and Function*. Mount Kisco, NY, Futura Publishing Co., inc. pp. 3-12.

Demuth, H.B., Beale, M., 1994, *Neural Network Toolbox User's Guide*. Natik, MA, The Mathworks, Inc.

Duda, R.O., Hart, P.E., 1973, *Pattern Classification and Scene Analysis*. New York, NY, John Wiley and Sons, Inc.

Evans, D.H., McDicken, W.N., Skidmore, R., Woodcock, J.P., 1989, *Doppler Ultrasound Physics, Instrumentation, and Clinical Applications*. New York, NY, John Wiley and Sons, Inc.

Gallagher, F.J., 1995, "Spectral Analysis of Fetal Blood Velocity in the Human", MS Thesis, Department of Mechanical Engineering, Rochester Institute of Technology, Rochester, New York.

Hagen, M.T., Demuth, H.B., Beale, M., 1996, *Neural Network Design*. Boston, MA, PWS Publishing Company.

Joern, H., Klein, A., Kuehlwein, H., Rath, W., 1997, "Critical Comparison of Indices and Threshold Values for Assessing Placenta Performance Using Doppler Ultrasound", *Ultrasound in Medicine and Biology*. Vol. 23 pp. 1179-1183.

Kempski, M.H., Kalegaonkar, S., Gallagher, F.J., Struijk, P.C., Ursem N.T.C., Wladimiroff, J.W., "Maternal-Fetal Doppler Velocity Reconstruction, Verification, and Variability Analysis", *Ultrasound in Medicine and Biology*, in review.

Laurin, J., Lingman, G., Marsal, Marsal, K., Persson, P., 1997, "Fetal Blood Flow in Pregnancies Coplicated by Interuterine Growth Retardation", *Obstetrics and Gynecology*. Vol. 69 pp. 895-902.

Marieb, E.N., 1991, *Human Anatomy and Physiology Second Edition*. Redwood City, CA, The Benjamin/Cumminings Publishing Co. inc. pp. 620-623.

Morrow, D.A., 1998, "Neural Network Applications in Signature Analysis", MS Paper, Department of Mechanical Engineering, Rochester Institute of Technology, Rochester, New York.

Sissman, N.J., 1970, "Developmental Landmarks in Cardiac Morphogenesis: Comparative Chronology", *American Journal of Cardiology*. Vol. 25 pp. 141-148.

Surat, D.R., Adamson, S.L., 1996, "Downstream Determinants of Pulsatility of the Mean Velocity Waveform in the Umbilical Artery as Predicted by a Computer Model", *Ultrasound in Medicine and Biology*. Vol. 26 pp.707-717.

Thompson, R.S., Stevens, R.J., 1989, "Mathematical Model for Interpretation of Doppler Velocity Waveform Indices", *Medical and Biological Engineering and Computing*. Vol. 27 pp. 269-276.

Thompson, R.S., Trudinger, B.J., 1989, "Doppler Waveform Pulsitility Index and Resistence, Pressure and Flow in the Umbilical Placental Circulation: An Investigation Using a Mathematical Model", *Ultrasound in Medicine and Biology*. Vol. 16 pp. 449-458.

Thompson, R.S., Trudinger, B.J., Cook, C.M., 1986, "A Comparison of Doppler Ultrasound Waveform Indices in the Umbilical Artery – I. Indices derived from the Maximum Velocity Waveform", *Ultrasound in Medicine and Biology*. Vol. 12 pp. 835-844.

Thompson, R.S., Trudinger, B.J., Cook, C.M., 1985, "Doppler Ultrasound Waveform in the Fetal Umbilical Artery: Quantitative Analysis Technique", *Ultrasound in Medicine and Biology*. Vol. 11 pp. 707-718.

Ursem, N.T.C., Brinkman, H.J.F, Struijk, P.C., Hop, W.C.J., Kempski, M.H., Keller, B.B., Waladimiroff, W., 1998, "Umbilical Artery Waveform Analysis Based on Maximum, Mean and Mode Velocity in Early Human Pregnancy", *Ultrasound in Medicine and Biology*. Vol. 24 pp. 1-7.

Wright, I.A., Gough, A.J., Rankebrandt, F., Wahab, M., Woodcock, J.P., 1997, "Neural Network Analysis of Doppler Ultrasound Blood Flow Signals: A Pilot Study", *Ultrasound in Medicine and Biology*. Vol. 23 pp. 683-690.

Appendix A
MATLAB Script Files

A.1 Trainer.m

```
%Modified by: Ron Soule July 22 1998
%
% Neural Network toolbox code to initialize, train, and sort results for a
% 5-N-2 logsig backpropagation network.
%
% Begin by loading training pairs (P,T) and proceed

clear
clc

AvgChar
[W1,b1,W2,b2]=initff(P,5,'logsig',2,'logsig');

disp_freq = 200;
max_epoch = 50000;
err_goal = 0.02;
lr = 0.2;
lr_incr = 1.04;
lr_decr = 0.7;
momentum = 0.9;
max_error_ratio = 1.04;

tp=[disp_freq max_epoch err_goal lr lr_incr lr_decr momentum max_error_ratio];

[W1,b1,W2,b2,te,tr] = trainbpx(W1,b1,'logsig',W2,b2,'logsig',P,T,tp);


save wab1 W1 b1 W2 b2
```

A.2 EvalNet.m

```
%Modified by: Ron Soule July 22 1998
%
% NN toolbox code for evaluation of a trained network.
% Begin by loading input (P,T) vectors to be evaluated
% Then, the evaluator will run it through most recently used trained
% network (which may need to be loaded).

[a2] = simuff(P,W1,b1,'logsig',W2,b2,'logsig');

% Now, sort through a2 to alter to nearest matching vector
% and compare to T

n = size (a2);
m = n(1) * n(2);
for ind = 1:m
  tmp = a2(ind);
                if tmp > 0.5
                        a2(ind) = 1.0000;
                else
                        a2(ind) = 0.0000;
    end
end
```

A.3 ComW10H

%Waveform index data (PI, AB ratio, RI, respectively), with target vectors used to train the Neural %Networks

```
P = [2.6054    16.42674    0.9391
     2.1319    6.5778      0.8467
     2.7197    18.17318    0.9449
     2.7373    17.5876     0.9428
     2.5511    18.48639    0.9458
     2.6788    15.49272    0.9352
     2.29      9.801049    0.8973
     2.3241    7.4597      0.8657
     2.3859    10.43858    0.9037
     2.4698    10.3942     0.9035
     2.5379    10.78524    0.907
     2.1683    7.430455    0.8652
     2.1616    7.23753     0.8615
     2.3893    10.50542    0.9047
     2.2375    9.57392     0.8937
     2.3225    8.2475      0.8783
     2.527     9.560941    0.8953
     2.3577    10.20766    0.9019
     2.706     21.46317    0.9529
     2.7128    15.07592    0.9336
     2.8132    20.01293    0.95
     2.7736    19.46906    0.9486
     2.8407    17.87028    0.9439
     2.4742    8.473273    0.8818
     2.3108    7.554143    0.8673
     2.4997    10.79034    0.9072
     2.3929    12.03739    0.9168
     2.0388    9.333141    0.8922
     2.2311    10.2768     0.8995
     2.2157    7.339067    0.8634
     2.4806    13.50805    0.9229
     2.4383    11.15381    0.9098
     2.0517    7.214324    0.8507
     2.7639    16.0565     0.9375
     2.3089    14.4801     0.9214
     2.7129    26.4187     0.9619
     2.487     13.9441     0.9281
     2.3399    11.20235    0.9076
     2.3885    14.9254     0.9306
     2.69394   21.0837     0.95103
     2.72319   20.7001     0.95153
```

```
    2.56123     15.7836     0.93654
    2.46575    13.6511      0.92605
    2.03258     7.1359      0.85941
    2.26306    10.6947      0.906210
    2.30542    10.91991     0.90832
    2.3281      8.386290    0.88045
    2.431       10.54654    0.90483
    2.0996      7.79472     0.87147];

P = P';

T = [ 0 0 0 0 0 0 0 0 0 0 0 0 0 0 0 0 0 0 0 0 0 0 0 0 0 0 0 0 0 0 0 0 1 1 1 1 1 1 1 1 1 1 1 1 1 1 1 1 1 1 1 1
      0 0 0 0 0 0 0 0 0 0 0 0 0 0 0 1 1 1 1 1 1 1 1 1 1 1 1 1 1 1 1 1 0 0 0 0 0 0 0 0 0 0 1 1 1 1 1 1 1 1 1 1];
```

A.4 Average.m

%A data set that contains the APV data for the four gestational weeks under investigation (the %colums represent the weeks of gestation). This set was used as training vectors.

```
P = [13.15204348    13.95490476  14.26247619  19.615
13.61065217  14.41309524  14.71661905  20.01744444
14.90595652  15.74957143  16.22814286  21.74666667
17.72308696  18.66180952  19.67571429  25.83644444
22.81043478  23.93247619  25.97804762  33.33733333
30.75617391  32.21428571  35.783       44.93288889
41.76886957  43.80847619  49.2132381   60.64044444
55.53443478  58.50109524  65.75409524  79.71488889
71.20004348  75.51561905  84.3172381   100.7842222
87.50526087  93.61152381  103.4556667  122.1651111
103.0307391  111.3094286  121.6567619  142.2411111
116.4854783  127.1802857  137.6268095  159.7823333
126.9516957  140.1105714  150.4909524  174.1144444
134.0163913  149.472619   159.8765238  185.1148889
137.767913   155.1642381  165.8811905  193.076
138.6758696  157.5300952  168.9494286  198.4986667
137.4127391  157.2019524  169.6990476  201.8927778
134.6723043  154.9127619  168.7472381  203.6426667
131.0331304  151.3309048  166.5870476  203.9598889
126.8829565  146.9505238  163.5322381  202.9226667
122.4059565  142.0582857  159.7269048  200.5598889
117.6207391  136.7638095  155.1916667  196.9243333
112.4503043  131.0600952  149.8864762  192.1206667
106.7907826  124.8862857  143.7715238  186.2868889
100.5652609  118.1751429  136.8467143  179.5622222
93.7516087   110.881      129.1581905  172.061
86.38869565  102.9902857  120.7787619  163.8648889
78.56769565  94.52628571  111.7840476  155.0224444
70.41726087  85.55742857  102.2544762  145.5612222
62.0903913   76.21347619  92.31042857  135.524
53.76408696  66.70619048  82.15980952  125.0326667
45.64830435  57.33442857  72.1222381   114.3368889
37.99347826  48.4642381   62.60404762  103.8075556
31.07565217  40.47861905  54.0212381   93.86677778
25.15656522  33.70652381  46.70347619  84.88577778
20.43217391  28.35390476  40.81790476  77.094
16.98486957  24.45880952  36.34266667  70.53933333
14.755       21.8857619   33.08947619  65.10311111
13.56604348  20.36290476  30.76419048  60.56011111
13.16356522  19.54957143  29.03857143  56.654
13.23908696  19.0877619   27.61657143  53.16133333
```

```
13.51913043  18.7547619   26.28261905  49.928
13.79673913  18.36061905  24.92214286  46.87722222
13.95        17.8412381   23.51514286  43.99911111
13.93978261  17.21428571  22.10947619  41.32955556
13.78878261  16.5342381   20.78080952  38.91711111
13.55591304  15.86352381  19.60009524  36.795
13.30491304  15.26342857  18.61104762  34.96288889
13.0983913   14.81580952  17.82633333  33.38733333
12.96447826  14.51671429  17.20761905  32.01755556
12.90247826  14.30209524  16.76080952  30.80088889
12.90391304  14.09342857  16.41919048  29.69
12.93821739  13.95990476  16.12742857  28.64888889
12.95882609  13.81366667  15.80652381  27.65566667];


T = [0 0 1 1
     0 1 0 1];
```

A.5 EVA.m

```
%The M-file to load the data files under investigation and run the various
%evaluation M-files

clear
clc

load wab1

j = 0;

Week10ch

EvalNet
figure(1)
  Hfig_1 = figure(1);
  set(Hfig_1, ...
  'NumberTitle', 'Off', ...
  'Name', ['Unknown']);

Ploti
Hold;
for i = 1:1
  j = j + 1;
end

Week11ch

EvalNet
Ploti
for i = 1:1
  j = j + 1;
end

Week12ch

EvalNet
Ploti
for i = 1:1
  j = j + 1;
end

Week13ch
EvalNet
Ploti
Hold;
```

A.6 Ploti.m

```
%Modified by: Ron Soule July 22 1998
%file to graphically represent how data is assigned


dim = size(a2);
xsize = dim(2);
x = [1:1:xsize];
for i = 1:xsize
        if a2(:,i) == [0 0]'
                step_loc(i) = 10;
        elseif a2(:,i) == [0 1]'
                step_loc(i) = 11;
        elseif a2(:,i) == [1,0]'
    step_loc(i) = 12;
  else
    step_loc(i) = 13;
        end
end

if j == 0
  plot(x,step_loc,'kx')
end

if j == 1
  plot(x+6,step_loc,'ok')
end

if j == 2
  plot(x+12,step_loc,'+k')
end

if j == 3
  plot(x+18,step_loc,'sk')
end


xlabel('Input Sample Number');
ylabel('Gestational Age (Weeks)');
legend('Week 10', 'Week 11', 'Week 12', 'Week 13');
axis([0 24 9.5 13.5]);
```

Appendix B

Complete Table of Fetal Pulse-Velocity Waveform Indices Used in Neural Network Training

Patient Number	Fetus Age	Day	S	D	M	PI	RI	AB	τ	
A03_0029UA2	Week 10	5	119.1332	9.8893	44.2533	2.4716	0.9169	12.0619	33.1574	N = 18
A04_0041UA2		1	180.0872	9.9012	62.5098	2.7197	0.9449	18.1732	39.9665	23 Total
A05_0058UA1		5	204.7626	10.0582	69.3908	2.8067	0.9509	20.5600	40.7755	
A05_0062UA2		2	176.7782	10.0464	60.8619	2.7373	0.9428	17.5876	39.1426	
A06_0076UA1		5	185.8611	10.0770	69.0643	2.5510	0.9459	18.4864	36.9351	
A06_0077UA1		6	152.9187	9.8913	53.5088	2.6788	0.9352	15.4927	40.8573	
A07_0089UA1		2	97.3331	9.9434	38.1155	2.2900	0.8973	9.8010	28.2097	
A09_0118UA1		4	111.6529	14.9538	41.5626	2.3241	0.8657	7.4597	28.8534	
A09_0120UA1		2	154.8480	14.8147	58.6028	2.3859	0.9037	10.4386	32.4167	
A10_0128UA1		3	123.2956	14.9439	47.8645	2.2630	0.8786	8.2480	30.3388	
A11_0142UA1		5	159.0871	14.7715	56.9553	2.5379	0.9070	10.7852	36.2698	
A13_0174UA1		0	111.1227	14.9621	44.3700	2.1684	0.8652	7.4305	29.0509	
A13_0177UA1		3	142.5648	19.7031	56.8555	2.1615	0.8615	7.2375	29.5799	
A14_0193UA1		0	206.0539	19.6320	78.1006	2.3893	0.9047	10.5054	30.6246	
A16_0214UA1		5	133.7193	14.8135	51.1128	2.3238	0.8887	9.0185	33.6077	
A20_0277UA1		3	123.2990	14.9490	46.6323	2.3225	0.8782	8.2475	29.5374	
A21_0296UA1		0	103.3412	15.0238	41.8145	2.1159	0.8542	6.9350	28.4271	
A22_0304UA1		3	142.0437	14.8422	50.2779	2.5271	0.8953	9.5609	32.6097	
Averaged Data		Test	145.9946	13.5120	53.9918	2.4319	0.9020	11.5572	33.3533	
A02_0010UA1	Week 11	2	119.8515	9.8655	44.0912	2.4950	0.9175	12.1513	38.3387	N = 15
A02_0022UA1		4	208.3984	9.7279	73.3789	2.7060	0.9529	21.4632	40.5871	20 Total
A04_0042UA3		2	148.0298	9.8199	50.9454	2.7128	0.9336	15.0759	39.6604	
A04_0043UA1		4	164.4324	9.8013	58.7335	2.6313	0.9391	16.7970	36.3422	
A05_0059UA1		4	198.6052	9.9278	67.0910	2.7982	0.9492	19.7225	39.5060	
A05_0061UA1		4	190.4777	9.7857	65.1546	2.7736	0.9486	19.4691	40.8506	
A06_0080UA1		4	176.9457	9.9044	58.8117	2.8407	0.9439	17.8703	38.1303	
A09_0116UA1		0	149.3983	19.7651	56.0596	2.3108	0.8673	7.5541	30.0773	
A11_0134UA1		1	130.3496	19.8774	53.5067	2.0632	0.8470	6.5539	26.1047	
A13_0168UA1		6	120.5461	10.0082	46.1582	2.3929	0.9167	12.0374	30.2677	
A15_0197UA2		3	183.3546	19.7307	80.2253	2.0388	0.8922	9.3331	32.3730	
A16_0223UA1		3	167.4884	16.8123	67.6785	2.2311	0.8995	10.2768	30.6636	
A18_0245UA1		5	189.3356	14.8688	68.7034	2.5365	0.9212	12.7212	33.5884	
A18_0247UA1		0	108.6797	14.8183	42.3931	2.2157	0.8634	7.3391	30.2468	
A18_0259UA1B		3	123.2029	18.3128	51.0935	2.0517	0.8506	7.2143	22.0383	
Averaged Data		Test	158.6064	13.5351	58.9350	2.4532	0.9095	13.0386	33.9183	
A03_0036UA1	Week 12	1	149.4401	11.7901	59.5937	2.3089	0.9214	14.4801	29.9827	N = 16
A04_0044UA1		5	140.2265	10.0623	52.2822	2.4870	0.9281	13.9441	36.0155	21 Total
A05_0057UA2		4	174.5048	12.0465	67.8727	2.3885	0.9307	14.9255	27.8215	
A05_0063UA1		1	221.5802	10.7807	78.0812	2.6939	0.9510	21.0838	35.5375	
A05_0065UA1		0	202.7163	9.7997	70.8905	2.7232	0.9515	20.7002	41.2687	
A07_0090UA2		1	232.2179	14.7106	84.9006	2.5612	0.9365	15.7836	36.2348	
A08_0101UA2		1	214.4168	15.8478	80.5198	2.4658	0.9261	13.6512	34.9033	
A09_0117UA2		0	209.6693	19.5965	83.9360	2.2631	0.9062	10.6948	28.2998	
A13_0170UA1		3	161.3410	14.7774	63.5703	2.3054	0.9083	10.9199	33.3245	
A13_0172UA1		1	165.3572	19.6939	62.4840	2.3282	0.8805	8.3863	31.4504	
A17_0234UA1		1	154.1973	19.7857	64.0219	2.0996	0.8715	7.7947	27.9108	
A17_0244UA1		2	209.5962	19.7175	85.1449	2.2288	0.9058	10.6288	32.7262	
A19_0264UA1B		0	177.1596	14.8125	69.4482	2.3360	0.9162	11.9536	29.8149	
A19_0269UA1B		0	176.0852	14.7592	64.0728	2.5216	0.9158	11.9463	31.9022	
A21_0285UA2		0	175.4742	17.6686	72.1653	2.1905	0.8984	10.3823	30.0144	
A21_0298UA1		2	158.7255	14.8109	57.1361	2.5183	0.9064	10.7149	32.7026	
Averaged Data		Test	182.6693	15.0412	69.7575	2.4012	0.9159	12.9994	32.4944	
A03_0028UA1	Week 13	1	181.5783	10.1753	68.3912	2.5038	0.9437	18.0391	35.1295	N = 5
A11_0137UA1		0	300.4831	19.7306	111.8883	2.5041	0.9341	15.2070	29.3820	9 Total
A13_0167UA1		0	164.2372	25.6657	75.4129	1.8383	0.8436	6.6528	25.5811	
A16_0221UA1		4	261.0049	19.7057	93.3860	2.5862	0.9245	13.2563	31.5688	
A18_0258UA1		5	302.7910	21.2370	121.1946	2.3268	0.9299	14.3757	27.8160	
Averaged Data		Test	242.0189	19.3029	94.0546	2.3518	0.9152	13.5062	29.8955	

Appendix C
Complete Set of Fetal Representative Pulse-Velocity Waveforms

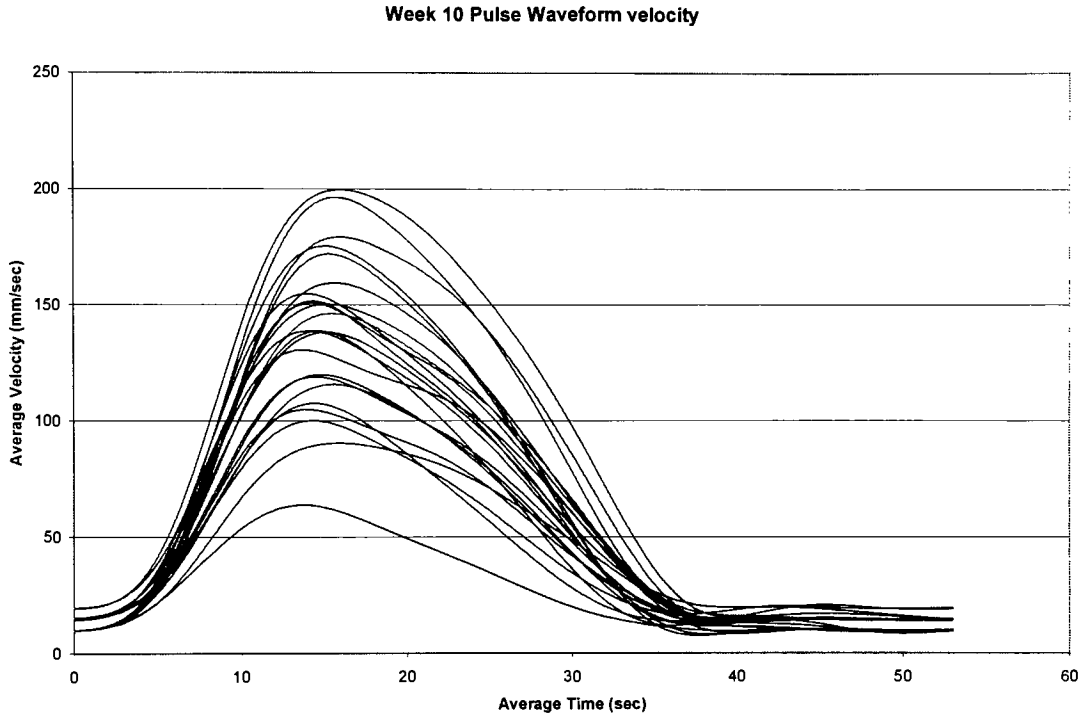

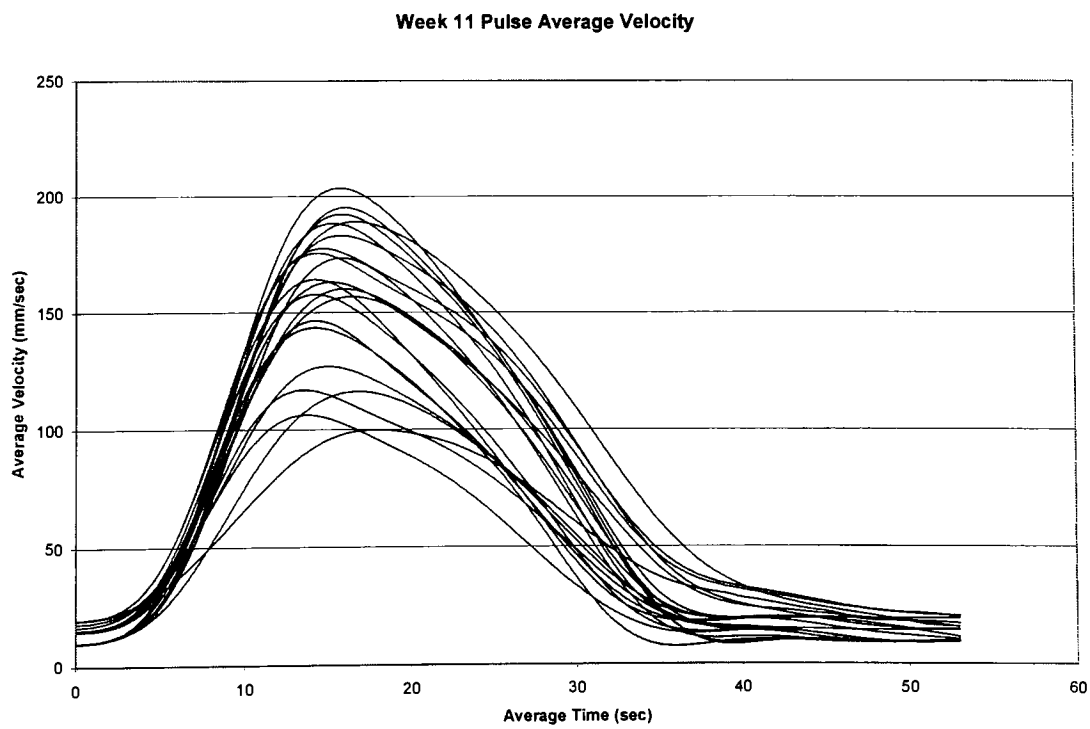

Week 12 Pulse Waveform Velocity

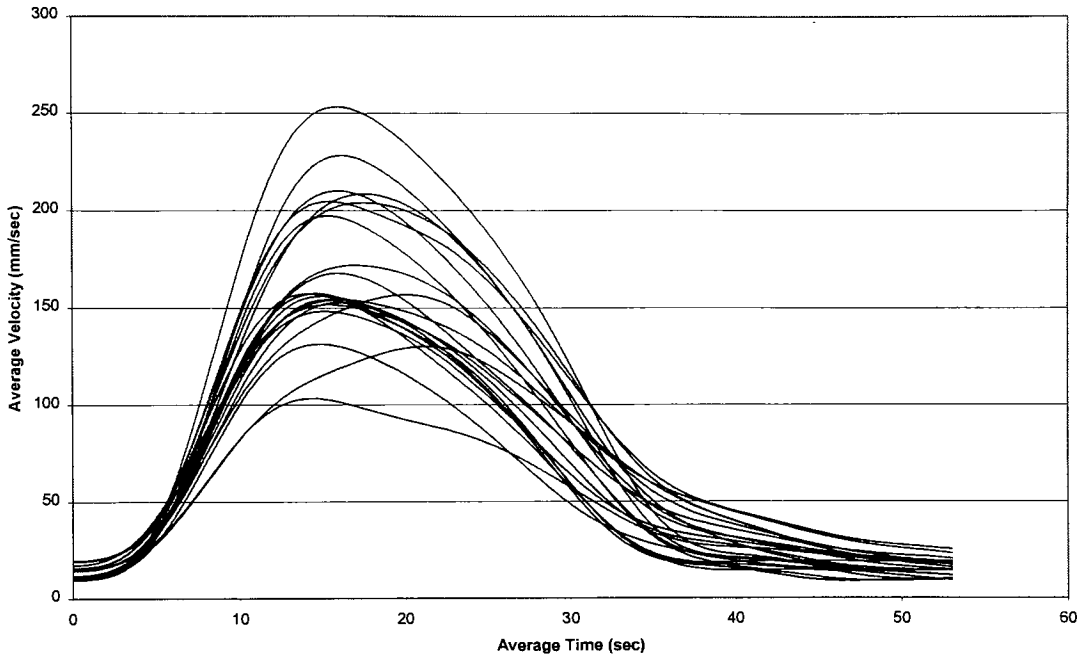

Week 13 Pulse Average Velocity

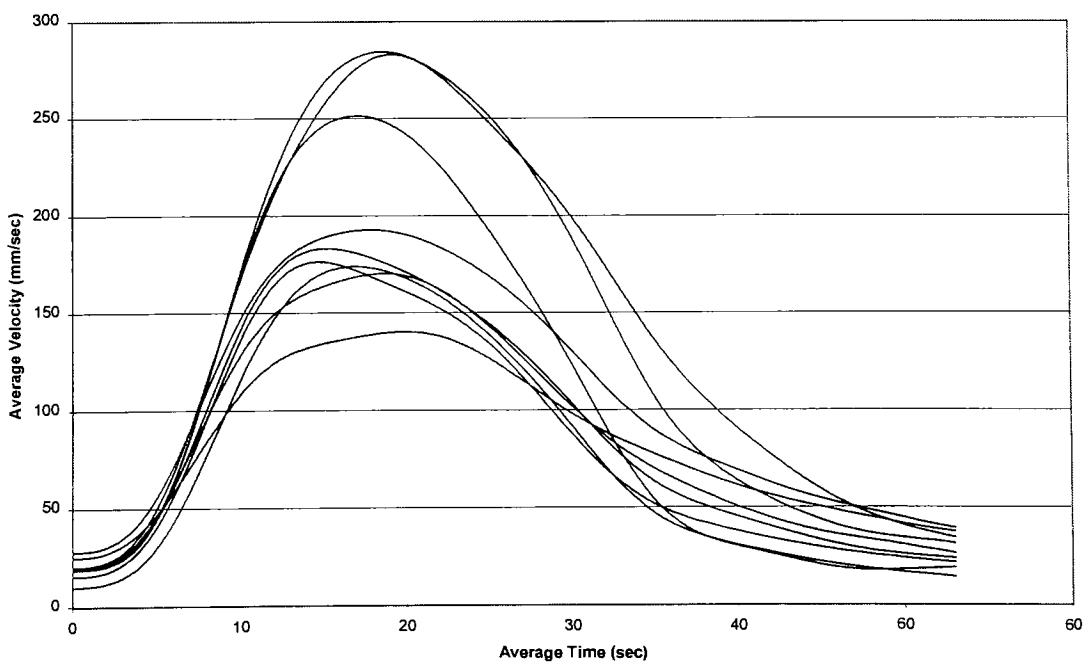

Appendix D
Fetal Week-Averaged Pulse-Velocity Waveforms with Confidence Intervals

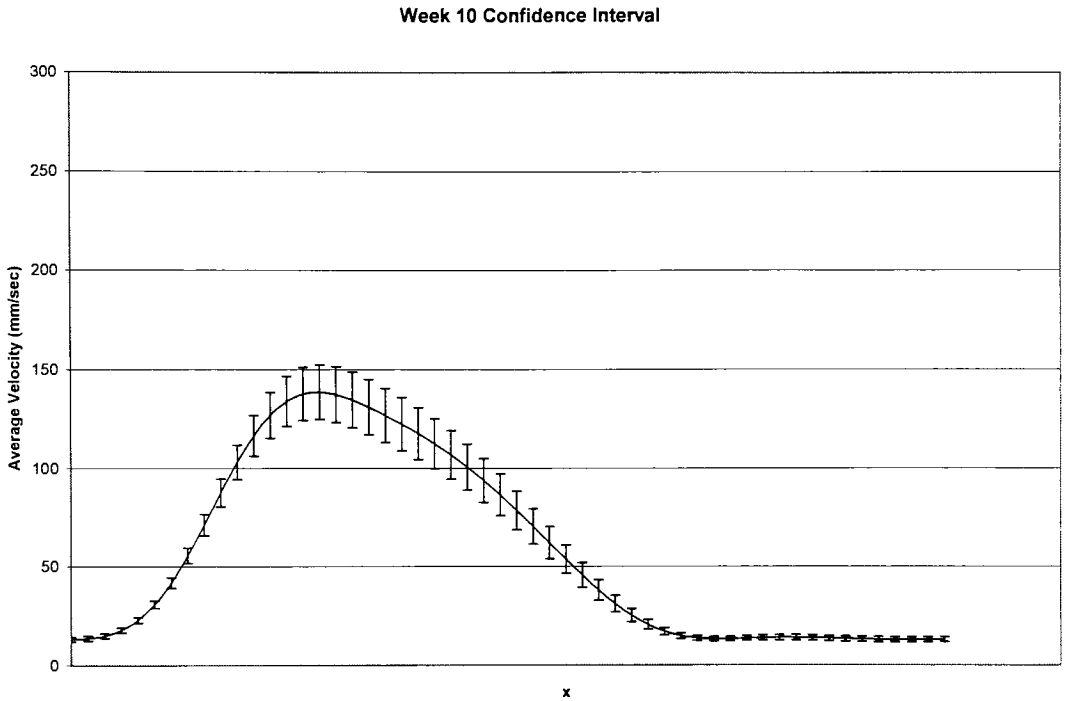

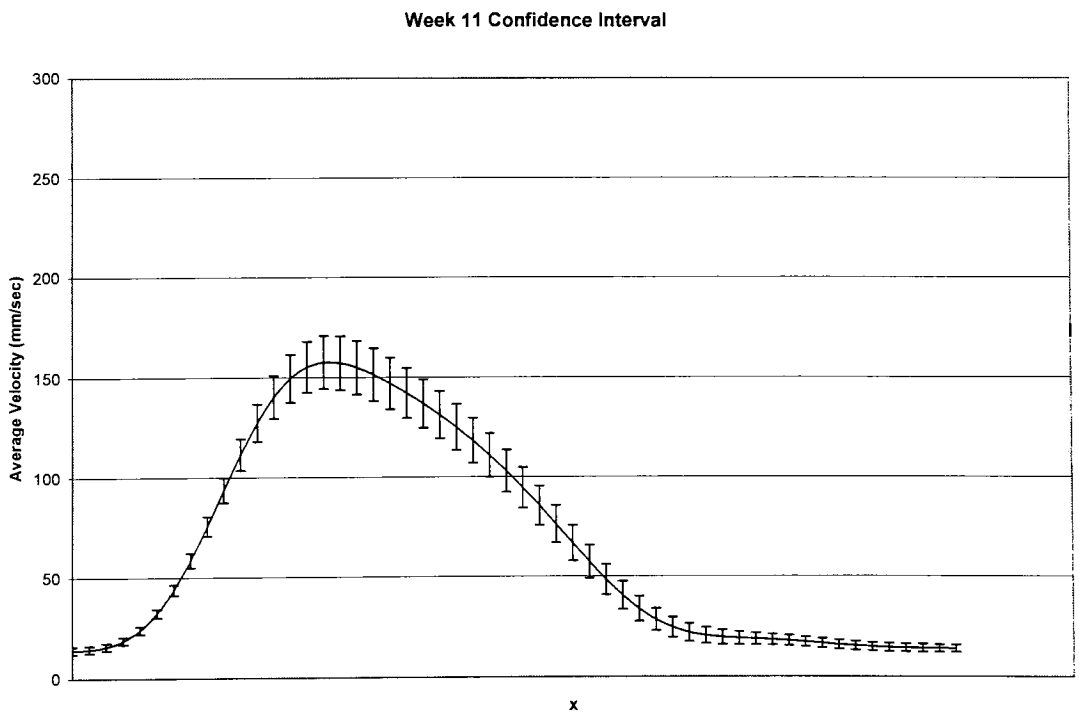

Week 12 Confidence Interval

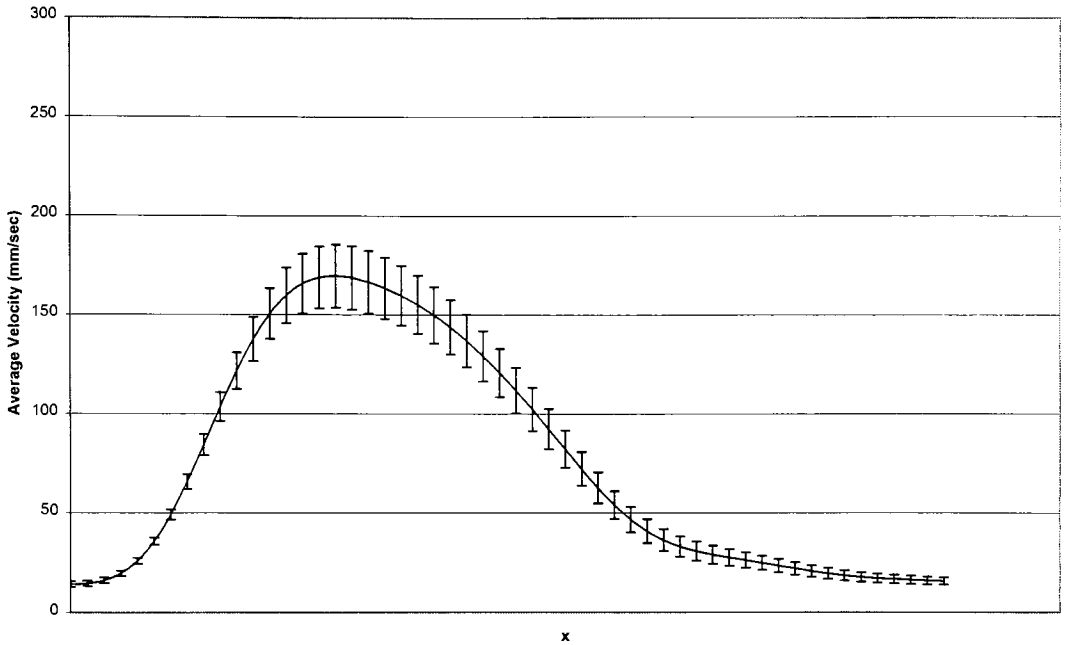

Week 13 Confidence Interval

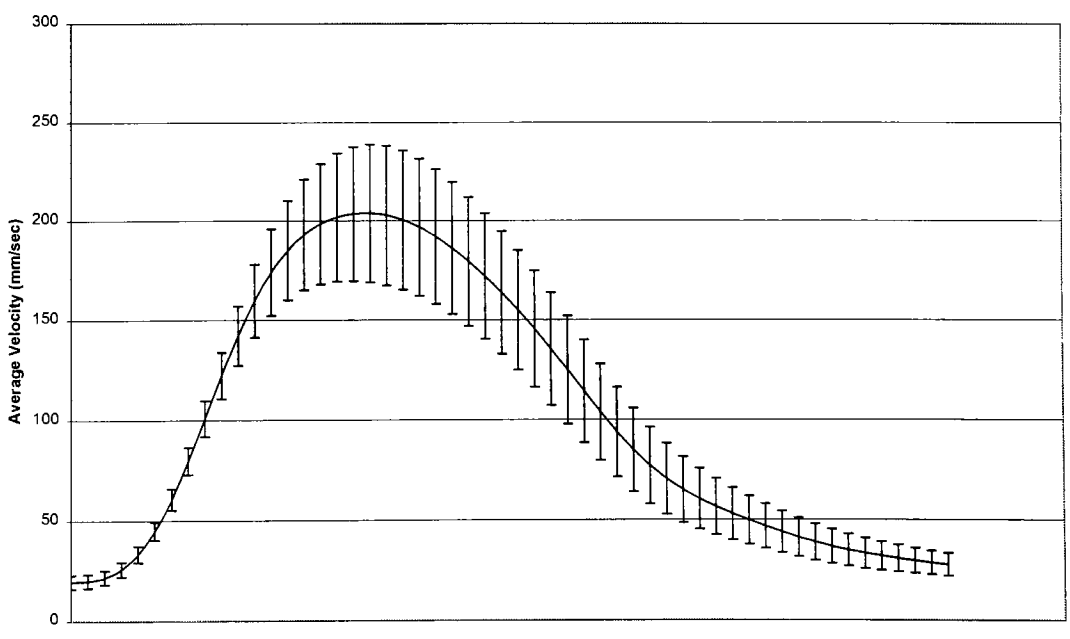

Weeks 11 & 12 Confidence Intervals

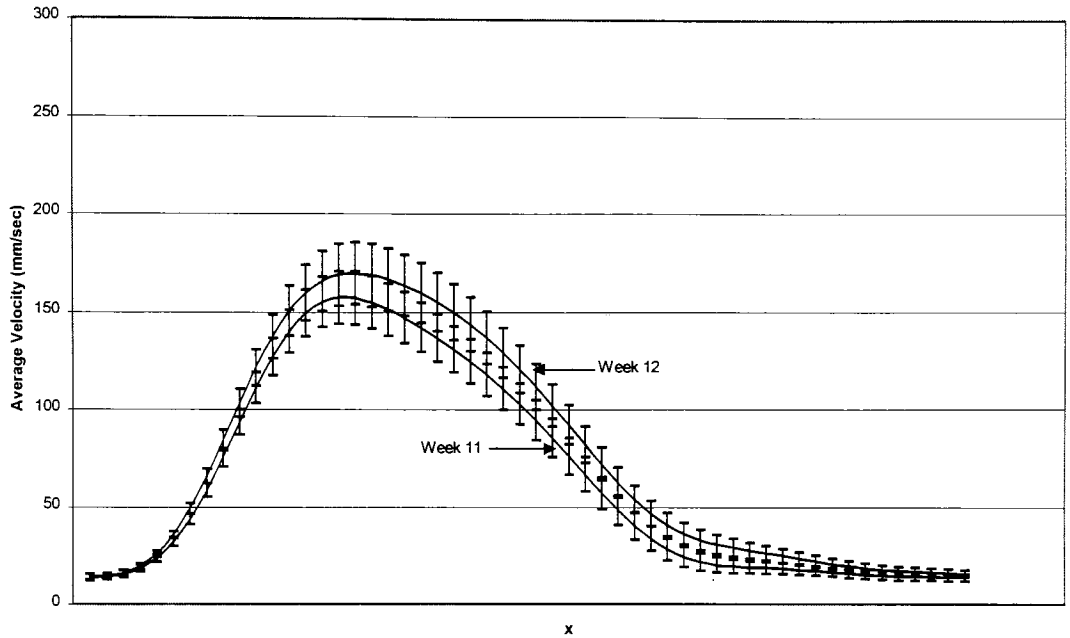

Weeks 10 & 11 Confidence Intervals

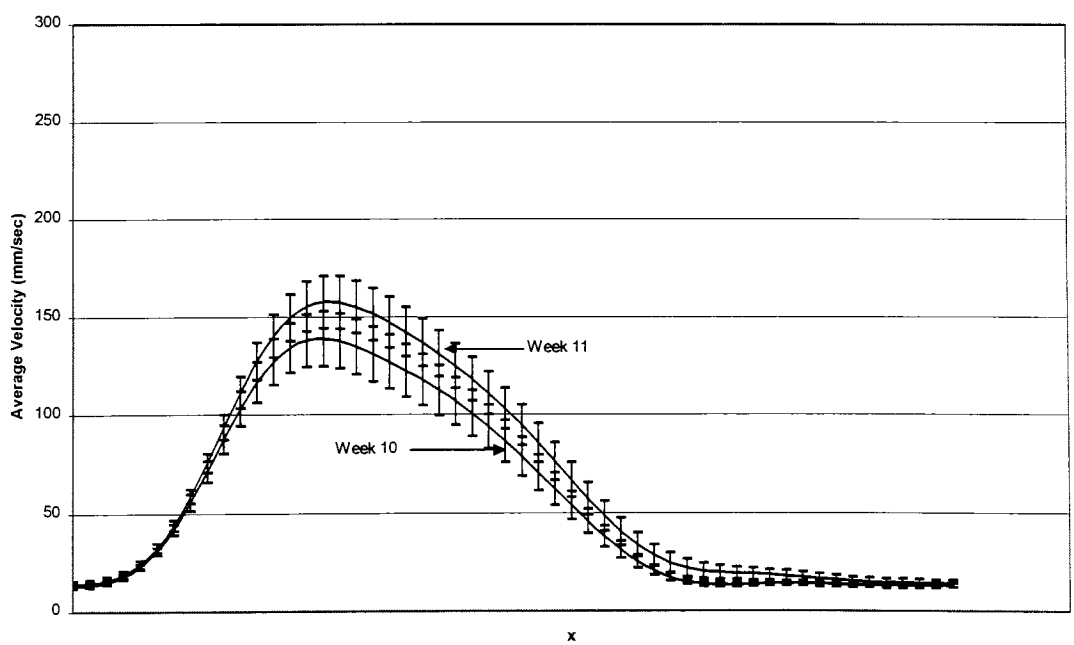

Weeks 12 & 13 Confidence Interval